

International Atomic Energy Agency

INDC(CCP)-402
Distrib.: G

INDC

INTERNATIONAL NUCLEAR DATA COMMITTEE

**SYSTEMATIC MEASUREMENT OF ACTIVATION CROSS
SECTIONS AT NEUTRON ENERGIES FROM 13.4-14.9 MeV**

A.A. Filatenkov, S.V. Chuvaev, V.N. Aksenov and V.A. Jakovlev

V.G. Khlopin Radium Institute
2nd Murinski Ave. 28, 194021, St. Petersburg, Russia

January 1997

IAEA NUCLEAR DATA SECTION, WAGRAMERSTRASSE 5, A-1400 VIENNA

Reproduced by the IAEA in Austria
January 1997

INDC(CCP)-402
Distrib.: G

**SYSTEMATIC MEASUREMENT OF ACTIVATION CROSS
SECTIONS AT NEUTRON ENERGIES FROM 13.4-14.9 MeV**

A.A. Filatenkov, S.V. Chuvaev, V.N. Aksenov and V.A. Jakovlev

V.G. Khlopin Radium Institute
2nd Murinski Ave. 28, 194021, St. Petersburg, Russia

Abstract

The results from systematic measurement of cross sections at neutron energies from 13.4-14.9 MeV for 70 activation reactions of importance for fusion and other applications are presented.

January 1997

SYSTEMATIC MEASUREMENT OF ACTIVATION CROSS SECTIONS AT NEUTRON ENERGIES FROM 13.4 -14.9 MeV *

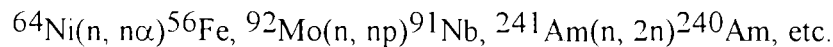
A.A.Filatenkov, S.V.Chuvaev, V.N.Aksenov, V.A.Jakovlev

V.G.Khlopin Radium Institute, St.Petersburg, RUSSIA

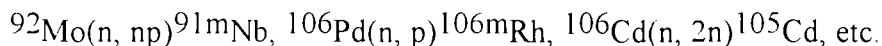
SYSTEMATIC MEASUREMENT OF ACTIVATION CROSS SECTIONS AT NEUTRON ENERGIES FROM 13.4 - 14.9 MeV. The results from the measurement of activation cross sections for 70 reactions of importance for fusion and other applications are presented.

1. INTRODUCTION

Cross sections of the reactions leading to material activation by neutrons with energies corresponding to the region of the D-T fusion neutron spectrum have been measured for a long time by many experimentalists. At present, there is a lot of data available, especially, in the region of neutron energy around 14 MeV. However, some unsolved problems still remain in this area. First, there are some reactions which are very important for fusion and applications but never have been measured satisfactorily. These are, for example,



Second, tens of reactions exist for which either the measurement was performed only once or a sharp disagreement between results of different experiments is observed. The urgent need is to repeat independently such measurements. Among these, the following reactions may be mentioned:



Finally, in spite of a great number of results that were obtained for reaction cross sections at neutron energies around 14 MeV, the evaluated data often have rather large uncertainties that exceed noticeably the attainable experimental errors. This is usually connected with a large scattering of data obtained by different authors.

The requests for new experimental data were discussed at many meetings that addressed various problems related to the peaceful application of atomic energy, such as the activation of structural materials, the generation of hydrogen and helium, tritium breeding, the delayed decay-heat of the reaction products, shielding problems, waste disposal, transmutation, etc. It was many times emphasized by specialists that increased accuracy of the basic data will lead to significant cost savings, for example, for the ITER Project, by reducing the engineering safety margins.

The purpose of the present work was the systematic and precise measurement of activation cross sections for some reactions of importance for fusion and other applications. Among them, special attention was paid to those reactions that were recommended to measure by IAEA Specialists.

* This work was supported in part by International Science and Technology Center (Project #176) and by International Atomic Energy Agency (Contract #8205)

Besides, starting the measurements, the authors aimed to prepare a broad experimental database that would permit making a new, more exact evaluation of reaction cross sections at neutron energies around 14 MeV, using the most modern results. Examples of such investigations are the systematic cross section measurement program that was recently completed with high accuracy for 190 reactions at JAERI (Japan) [1, 2], and measurements for 58 reactions performed at IAE (China) [3].

In the experiment carried out at the Khlopin Radium Institute, the conventional methods were modernized. This enabled a high accuracy for activation cross sections to be achieved in spite of the rather modest parameters of the Neutron Generator NG-400. Measurements were started in 1989 but were practically stopped in the beginning of 1992 due to a lack of finances and were then continued only at the end of 1994 after signing of corresponding contracts with IAEA and ISTC. To date, more than 400 differential cross sections have been measured for 70 reactions. The main cycle of measurements is planned to be completed in 1997. In the present paper the experimental method is described, and the measurement results are presented for those cross sections where the data processing is already finished.

2. EXPERIMENTAL METHOD

Activation cross section measurements were carried out using a conventional, widely used scheme: irradiation - cooling - gamma counting. Briefly, the main features of the measurement procedure are as follows:

a) most of the reaction cross sections were measured at 7 or 8 neutron energy values in the interval 13.4-14.9 MeV for rigidly fixed standard conditions. To increase the reliability of these results, some standard reactions known with accuracy of 1.5 - 3%, were measured for the same conditions;

b) the scattered neutron contribution was minimized by the use of thin-wall constructions and air cooling of the target;

c) for neutron fluence determination, two reference reactions were used simultaneously, namely, the $^{27}\text{Al}(n, \alpha)^{24}\text{Na}$ and the $^{93}\text{Nb}(n, 2n)^{92\text{m}}\text{Nb}$, that are known with accuracy 0.5 - 2.5%;

d) the neutron flux was measured using the scanning scintillation detector that worked on-line with a PC. This allowed continuous monitoring of both angular and energy distributions of neutrons during irradiations;

e) the neutron field parameters were also calculated in detail. For this, a special code was written that took into account the real properties of the target and the real geometry of experiment.

f) accumulation, treatment and presentation of the data were fully computerized. The complete information about the measurements is stored in a structured data bank that was provided with service codes.

g) some effort was made to prepare a handbook on activation data in electronic format. At present, this handbook includes activation cross sections for about 4000 reactions, binding energies for about 3000 nuclei and data on approximately 15000 gamma rays from 2777 decays.

Below, these issues are considered in more detail.

The irradiation arrangement is shown in Fig. 2.1. The samples were gathered into assemblies that were mounted relative to the beam direction at the angles of 0, 40, 60, 80, 100, 120 and 140 degrees (the ring No. 1 for seven assemblies) and at 0, 40, 60, 75, 91, 107, 125 and

150 degrees (the ring No. 2 for eight assemblies). The distance from the center of the target to the centers of the front foils was 30 mm. In this arrangement, the neutron energy interval 13.4 - 14.9 MeV was covered when the D-T neutrons were used.

Special attention was paid to minimizing the contribution of scattered neutrons to the primary neutron spectrum. The target chamber and the sample holders used in the irradiations had thin walls with thickness of only 0.25 - 0.5 mm (see Fig. 2.1). The thickness of the sample packets varied from 1.5 to 5 mm. The distance between the target and the samples was much less than the distance between the target and the thick concrete walls of the experimental hall (3 cm and 150-1000 cm respectively). As a result, the fraction of scattered neutrons inside the samples was as low as 1 - 2%.

The $^{93}\text{Nb}(n, 2n)^{92\text{m}}\text{Nb}$ reaction was used as the primary standard for neutron fluence determination. This reaction has some properties that make it very suitable for this purpose. Among them, a small, no more than 5%, change of cross section over the neutron energy interval 13.5 - 14.9 MeV, and an almost optimal half-life of $^{92\text{m}}\text{Nb}$ (10.2 d) which does not require large corrections for decay during irradiation but, on the other hand, allow re-use of samples after 2 - 3 months of cooling.

Typically, 2 - 4 different materials were irradiated simultaneously. The samples were gathered in packets in which the first and the last position were occupied by the Nb foils. This permitted reliable interpolation of neutron flux that varied inside the assembly from sample to sample. Moreover, the fixed geometry of irradiation allowed to use 14 (for 7 sample positions) or 16 (for 8 sample positions) values of the neutron fluence deduced by Nb monitor foils for the calculation of neutron fluence accumulated by a sample. This reduced the uncorrelated part of errors by a factor approximately 2.5 in comparison with the conventional method where the fluence is determined independently for each assembly.

In addition, Al foils were placed in the middle of each packet. They were used to improve the accuracy of the absolute neutron flux determination, because the $^{27}\text{Al}(n, \alpha)^{24}\text{Na}$ cross section is known with high precision.

Variations of neutron flux during irradiation were measured by two independent scintillation detectors, one of which was fixed rigidly and the other was rotated around the target, at the distance 1 m, over the angular range -160 to +120 degrees. A standard period of 20 s was set for a rotation cycle, however, if necessary, that could be changed from 5 s to 2 min.

Three parameters were determined by this scanning scintillation detector for each event pulse: angle, amplitude and time of flight. The data were accumulated event by event in a buffer that was sorted to the relevant arrays at the moment when the detector changed the direction of movement at the backmost position. Detailed information on the angular and energy distribution of neutrons, and their variations during the irradiation, was written periodically to the PC disk and this was used then in the data processing.

The induced gamma activity was counted by a large volume Ge(Li) detector. Its efficiency was measured at different distances using standard gamma sources (OSGI) as well as other radioactive nuclides produced at the Neutron Generator. The efficiency dependence on energy and distance were approximated by analytical formulas. At the standard distance between sample and detector, which was 33 mm from the upper surface of detector to the lower side of the sample, the absolute efficiency of the detector was 0.992% for $E_\gamma = 661.6$ keV and 0.506% for $E_\gamma = 1332.5$ keV. The detector was secluded in a heavy shield consisting of consecutive layers of lead, cadmium and steel. This provided a background level as low as 0.00018 counts/s/keV at a gamma energy about 1330 keV. The count rate for the most intense background peak (due to ^{40}K) was 0.0048 counts/s.

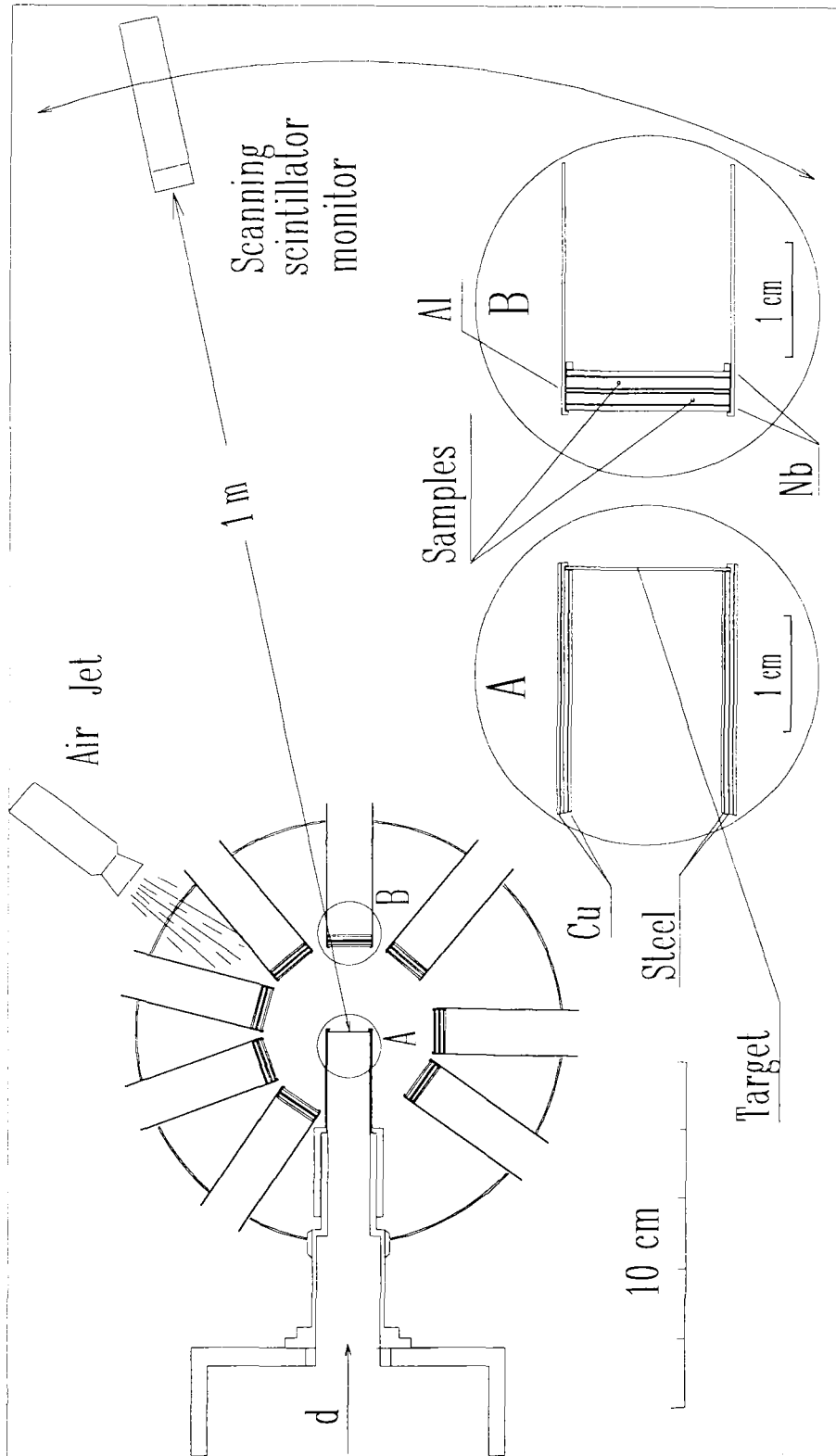


Fig. 2.1. Near target arrangement at the irradiation.

The data treatment included gamma spectra processing, peak identification, calculation of the induced activity of the sample, neutron flux determination and calculation of the activation cross section. For this, a packet of programs was written in TURBO PASCAL 7.0. It operated on a structured data bank of the experimental and reference data. This allowed recalculation of any cross section very quickly if some new information appeared, for example, about the reference data.

A special electronic handbook was created to make the job of preliminary data analysis, and preparation for new measurements, more productive and comfortable. By means of this, a great variety of information could be retrieved quickly, such as isotopic abundance of natural materials, reaction thresholds, expected cross sections, half-lives of reaction products, gamma ray energies and yields, interfering reactions, etc. At present, this electronic handbook works with databases that contain information on binding energies for about 3000 nuclei [4], approximately 4000 reaction cross sections [5], and about 15000 gamma rays from 2777 decays [6]. It is governed through a choice of 19 menu items that may be linked in various combination using logical conditions AND, OR and NOT. Although the handbook was created to service a rather special task, nevertheless, it seems to be able to meet various requests of specialists working in other areas of nuclear physics.

The decay data of isotopes that were involved in the process of cross section calculation for the present study are presented in Table 2.1. If several gamma lines of an isotope were observed in the experiment, then the cross section was deduced as the mean weighted value for all observed gamma peaks.

Table 2.1. Decay data used in this work.

Nucleus	T _{1/2}	E _γ [keV]	Y _γ [%]
²² Na	2.6088(14) y	1274.5	99.944(14)
²⁴ Na	14.9590(12) h	1368.6	99.99(1)
		2754.0	99.88(1)
²⁷ Mg	9.458(11) m	843.76	73.10(1)
		1014.4	28.50(1)
³⁸ Cl	37.24(5) m	1642.7	31.0 (10)
		2167.6	42.0 (30)
⁴¹ Ar	109.34(12) m	1293.1	99.10(1)
³⁸ K	7.636(18) m	2167.6	99.87(2)
⁴⁸ Sc	43.67(9) h	983.5	100.1(3)
		1037.5	97.6(7)
		1312.1	100.1(7)
⁵² V	3.743(5) m	1434.1	100.00(15)
⁵⁴ Mn	312.12(10) d	834.8	99.976(1)
⁵⁶ Mn	2.5785(2) h	846.8	98.87(3)
		1810.7	27.19(80)
		2113.0	14.34(40)
⁵⁹ Fe	44.503(6) d	192.4	3.08(12)
		1099.3	56.5(19)
		1291.5	43.2(14)
⁵⁷ Co	271.79(9) d	122.1	85.60(17)
		136.5	10.68(8)
^{58g} Co	70.82(3) d	810.8	99.448(8)

⁶⁰ Co	1925.1(5) d	1173.2	99.9736(7)
		1332.5	99.9856(4)
⁵⁷ Ni	35.60(6) h	127.2	16.66(3)
		1377.6	81.7(2)
		1919.5	15.0(3)
⁶⁵ Ni	2.5172(3) h	366.3	4.805(60)
		1115.5	15.43(14)
		1482.0	23.59(14)
⁶⁴ Cu	12.700(2) h	1345.8	0.473(10)
^{85m} Kr	4.480(8) h	151.2	75.4(18)
		304.9	14.0(4)
^{86m} Rb	1.017(3) m	556.07	98.17(9)
^{86g} Rb	18.631(18) d	1077.0	8.64(4)
^{87m} Sr	2.827(1) h	388.5	81.9(5)
⁹¹ Sr	9.63(5) h	555.6	56.11(10)
		749.8	23.6(5)
		1024.3	33.4(5)
⁸⁸ Y	106.65(4) d	898.0	93.7(3)
		1836.1	99.2(3)
^{90m} Y	3.244(5) h	202.1	97.3(4)
		479.5	90.74(5)
⁹² Y	3.54(1) h	934.5	13.9(13)
		2339.9	4.78(2)
^{89m} Zr	4.18(1) m	587.8	89.50(5)
		1507.3	6.04(7)

^{89g} Zr	78.41(12) h	909.1	99.871(3)
⁹⁵ Zr	64.02(5) d	724.2	44.17(15)
		756.7	54.46(10)
^{92m} Nb	10.15(2) d	912.6	1.8(1)
		934.2	99.07(4)
^{91m} Mo	65.0(7) s	652.9	48.2(13)
		1208.1	18.78 (58)
		1508.0	24.40 (73)
¹⁰³ Ru	39.26(2) d	497.1	91 (3)
¹⁰⁵ Ru	4.44(2) h	469.4	17.5(6)
		676.4	15.7(5)
^{106m} Rh	131(2) m	429.4	13.3(21)
		450.8	24.2(13)
		616.1	20.2(14)
		717.2	28.9(16)
		748.5	19.3(11)
		825.0	13.6(8)
		1046.7	30.4(16)
		1127.7	13.7(9)
¹⁰¹ Pd	8.47(6) h	269.7	6.4(4)
		296.3	19.2(10)
		590.4	12.1(7)
		1289.0	2.28(14)
^{106m} Ag	8.28(2) d	406.2	13.42(30)
		429.6	13.15(30)
		451.0	28.23(70)
		616.2	21.57(60)
		717.3	28.94(80)
		748.4	20.61(60)
		824.7	15.34(50)
		1045.8	29.55(100)
^{108m} Ag	418(21) y	1128.0	11.75(50)
		1199.4	11.22(30)
		1527.7	16.31(50)
¹¹² Ag	3.130(9) h	433.9	90.5(6)
		614.3	89.8(19)
		722.9	90.8(19)
¹⁰⁵ Cd	55.5(4) m	606.2	3.51(10)
		617.0	42.80(20)
		346.9	4.20(40)
		433.2	2.81(20)
		607.2	3.74(30)
^{111m} Cd	48.54(5) m	961.8	4.69(30)
		1302.5	3.97(30)
		1388.5	2.70(20)
		1693.3	3.53(30)
^{115m} Cd	44.6(3) d	150.8	29.1(3)
		245.4	94.0(5)
^{115g} Cd	53.46(10) h	933.8	2.0(7)
		336.2	45.9(2)
		492.6	8.03(10)
		527.9	27.5(2)

^{113m} In	1.6582(6) h	391.7	64.2(8)
^{114m} In	49.51(1) d	190.5	15.6(7)
		558.0	4.39(20)
		725.2	4.33(20)
		1300.0	0.19(3)
^{115m} In	4.486(4) h	336.2	45.79(10)
^{135m} Xe	15.29(5) m	526.5	80.5(5)
^{135g} Xe	9.14(2) h	249.8	90.5(5)
		608.6	2.38(5)
¹³⁷ Cs	30.07(3) y	661.6	85.1(1)
^{137m} Ba	2.552(1) m	661.6	90.11(6)
^{148m} Pm	41.29(11) d	550.1	94.55(90)
		629.9	88.6(7)
		725.6	32.69(30)
¹⁴⁹ Eu	93.1(4) d	277.1	3.56(6)
		327.0	4.03(12)
^{150m} Eu	12.8(1) h	333.9	3.85(10)
		406.5	2.73(10)
		831.8	0.23(5)
		921.7	0.27(5)
		1165.7	0.24(5)
^{150g} Eu	36.9(9) y	334.0	96.0(30)
		439.4	80.4(30)
		505.5	4.8(2)
		584.3	52.6(25)
		734.4	9.6(3)
		748.0	5.2(2)
^{152m1} Eu	9.3116(13) h	1049.0	5.4(2)
		121.8	7.21(90)
		344.3	2.44(30)
		562.9	0.23(3)
		841.6	14.60(21)
		963.3	12.10(20)
		1314.7	0.95(13)
¹⁵² Eu	13.573(5) y	1389.0	0.70(20)
		121.8	28.40(23)
		344.3	26.60(9)
		778.9	12.96(7)
		964.1	14.62(6)
		1112.1	13.54(6)
²⁰³ Pb	51.873(9) h	1408.0	20.85(8)
		279.19	80.8(2)
		401.3	3.46(17)
		680.5	0.70(8)
²³⁷ U	6.75(1) d	208.0	21.14(23)
²³⁹ Am	11.9(1) h	226.4	3.3(2)
		228.2	11.3(6)
		277.6	15.0(7)
²⁴⁰ Am	50.8(3) h	888.8	25.1(4)
		987.6	73.2(10)

As was mentioned above, the primary reference reaction cross section in the entire experiment was the cross section of the $^{93}\text{Nb}(n, 2n)^{92\text{m}}\text{Nb}$. At the beginning, it was supposed that it invariant with neutron energy over the range 13.4 - 14.9 MeV, and equal to 460 mb. This proposal corresponded to the evaluations available at that time [7, 8]. The uncertainty of these evaluations was 1.1% at 14.5 MeV neutron energy and it increased to 1.5 - 2.3% at the endpoints of the interval 13.4 - 14.9 MeV. Using the large volume of data obtained in this experiment, it was possible to improve the accuracy of the primary reference cross section. For this, use was made of the $^{27}\text{Al}(n, \alpha)^{24}\text{Na}$ reaction for which the cross section is known with an accuracy of 0.3 - 0.6%. Experimental mean weighted values of this cross section, (obtained) on the assumption of a the constant value 460 mb for the $^{93}\text{Nb}(n, 2n)^{92\text{m}}\text{Nb}$ cross section, were then normalized to the EAF-4 evaluation for the $^{27}\text{Al}(n, \alpha)^{24}\text{Na}$. This is shown in Figure 2.2. Then, the resultant bias factors were used to correct the $^{93}\text{Nb}(n, 2n)^{92\text{m}}\text{Nb}$ cross section. The result is shown in Fig. 2.3. The cross section was altered by no more then 2% (at neutron energy 13.47 MeV). These primary cross sections were then used as the reference values for calculation of all other cross sections obtained in the present work. The digital values of the primary cross sections used in this paper are given in the Table 2.2. Characteristics of the samples used are presented in Table 2.3. In the cases when powder materials were used, these samples were pressed into tablets of standard sizes.

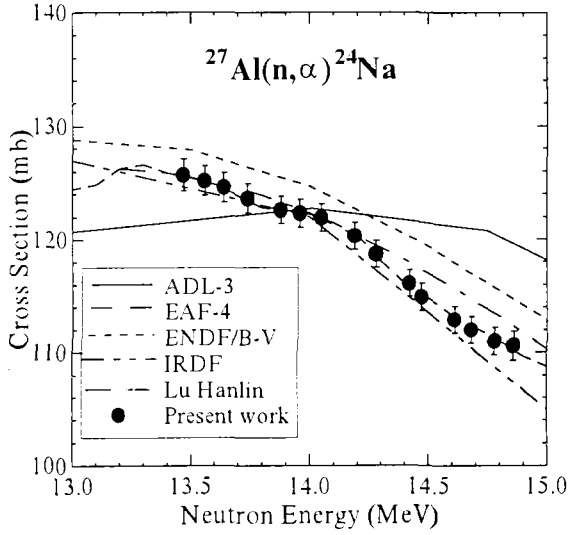


Fig. 2.2. Cross section data of $^{27}\text{Al}(n, \alpha)^{24}\text{Na}$.

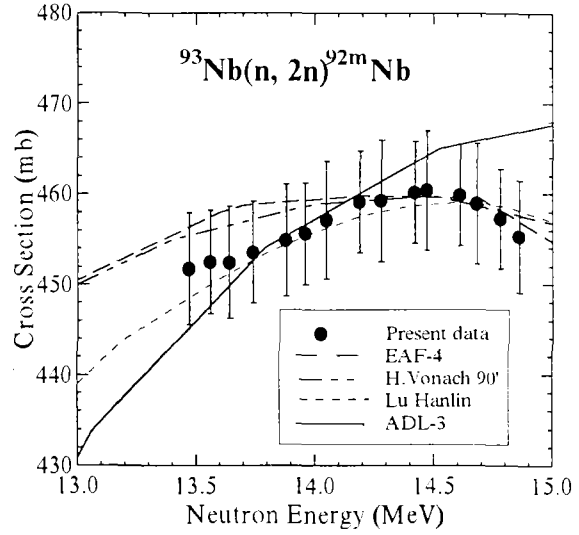


Fig. 2.3. Cross section data of $^{93}\text{Nb}(n, 2n)^{92m}\text{Nb}$.

Table 2.2. Cross section data for the $^{27}\text{Al}(n, \alpha)^{24}\text{Na}$ and $^{93}\text{Nb}(n, 2n)^{92m}\text{Nb}$ reactions which were used in the present work as reference values.

E_n , (MeV)	Cross section (mb)	
	$^{27}\text{Al}(n, \alpha)^{24}\text{Na}$	$^{93}\text{Nb}(n, 2n)^{92m}\text{Nb}$
13.47	125.7 (1.4)	451.7 (6.2)
13.56	125.2 (1.3)	452.4 (5.7)
13.64	124.6 (1.3)	452.4 (6.2)
13.74	123.6 (1.3)	453.6 (5.6)
13.88	122.6 (1.2)	454.9 (6.2)
13.96	122.3 (1.2)	455.6 (5.6)
14.05	121.9 (1.2)	457.1 (6.5)
14.19	120.3 (1.2)	459.1 (5.6)
14.28	118.7 (1.2)	459.2 (6.7)
14.42	116.1 (1.2)	460.2 (5.6)
14.47	114.9 (1.2)	460.4 (6.6)
14.61	112.9 (1.2)	459.9 (5.6)
14.68	112.0 (1.2)	458.9 (6.7)
14.78	111.0 (1.2)	457.3 (5.5)
14.86	110.6 (1.3)	455.3 (6.2)

The uncertainties expressed in milibarns are shown in the brackets.

Table 2.3. List of chemical properties, weights and abundances of samples.

Target nucleus	Chemical form	Physical form	Weight (mg)	Abundance (%)
²³ Na	NaCl	powder	900	100
²⁷ Al	Al	metal	90	100
³⁹ K	KNO ₃	powder	1250	93.2584(44)
⁴¹ K	KNO ₃	powder	1250	93.2584(44)
⁵¹ V	V	metal	450	99.750(2)
⁵⁵ Mn	KMnO ₄	powder	1100	100
⁵⁶ Fe	Fe	metal	450	91.754(36)
⁵⁹ Co	Co	metal	400	100
⁵⁸ Ni *	Ni	metal	100	99.8(1)
⁶⁰ Ni	Ni	metal	400	26.223(8)
⁶³ Cu	Cu	metal	360	69.13(3)
⁶⁵ Cu	Cu	metal	360	30.83(3)
⁸⁸ Sr *	SrCO ₃	powder	800	99.94(3)
⁸⁹ Y	Y	metal	70	100
⁹⁰ Zr	Zr	metal	300	51.45(3)
⁹² Zr	Zr	metal	300	17.15(2)
⁹⁴ Zr	Zr	metal	300	17.38(4)
⁹⁶ Zr	Zr	metal	300	2.80(2)
⁹³ Nb	Nb	metal	180	100
⁹² Mo	Mo	metal	900	14.84(4)
¹⁰² Pd	Pd	metal	250	1.02(1)
¹⁰⁶ Pd	Pd	metal	250	27.33(3)
¹⁰⁸ Pd	Pd	metal	250	26.46(9)
¹⁰⁷ Ag	Ag	metal	150	51.839(7)
¹⁰⁹ Ag *	Ag	powder	1200	99.4((1)
¹⁰⁶ Cd	Cd	metal	700	1.24(4)
¹¹² Cd	Cd	metal	700	24.13(14)
¹¹⁶ Cd	Cd	metal	700	7.49(12)
¹¹³ In	In	metal	500	4.29(2)
¹¹⁵ In *	In	metal	450	99.98(4)
¹³⁸ Ba *	BaCO ₃	powder	1500	99.8(1)
¹⁵¹ Eu *	Eu ₂ O ₃	powder	650	97.5(1)
¹⁵³ Eu *	Eu ₂ O ₃	powder	1000	99.2(8)
²⁰⁴ Pb	Pb	metal	1000	1.4(1)
²³⁸ U	U	metal	2300	99.2745(15)
²⁴¹ Am *	Am(NO ₃) ₃	solution	2.6	99.9

* - Separated isotope were used

3. BASIC ALGORITHM FOR DETERMINATION OF ACTIVATION CROSS SECTIONS

By definition, the cross section of the nuclear reaction $\mathbf{A}(n, \mathbf{x})\mathbf{B}$ is determined by the relation:

$$\sigma_{AB} = \frac{N_B}{N_A \cdot \Phi_n}, \quad (3.1)$$

where N_B is the number of nuclei \mathbf{B} produced in the reaction and N_A is the number of target nuclei \mathbf{A} ; Φ_n is the fluence of the particles that induce the reaction. Now, consider the procedures used to determine each of the three values in the formula (3.1).

3.1. Determination of target nuclei number

The number of the initial nuclei, N_A , is connected with the mass of the sample through:

$$N_A = \frac{m \cdot Aw \cdot p_1 \cdot p_2}{At}, \quad (3.2)$$

where m is the sample mass, g;

Aw is the Avogadro's number;

p_1 is the abundance of the isotope A in the chemical element;

p_2 is the share of the chemical elements in the chemical formula;

At is the atomic weight of atoms of the sample, a.e.m;

3.2. Neutron fluence determination

There are several methods used to measure integrated flux. The approach used in this work involves the use of ratios. Then, many factors cancel diminishing the total uncertainty of the data.

In this approach, the integrated neutron fluence accumulated by the reference sample is determined as

$$\Phi_n = \frac{N_{rB}}{N_{rA} \cdot \sigma_{rAB}}, \quad (3.3)$$

where the formula is similar to (3.1) and "r" means "reference". Usually, σ_{rAB} is known with good accuracy; N_{rA} and N_{rB} should be determined by the same procedures as N_A and N_B .

The fluence accumulated by each sample depends on the sample position in the assembly. This dependence is described well by the $1/r^2$ -law if the neutron scattering and size of sample and target are neglected. For the realistic conditions of the experiment (the target-sample distance is 30 mm, beam diameter 5 mm, diameter of the sample 14 mm, and sample thickness 0.3 mm), the neutron fluence dependence on distance is approximated by the same law rather well because the effects of neutron scattering and finite size remain small and have opposite signs. To simplify

the following formulas one can introduce a new variable, the so called "reverse fluence", φ_n , that is connected with the fluence Φ_n by:

$$\varphi_n = \frac{1}{\sqrt{\Phi_n}} \quad (3.4)$$

Then the reverse fluence φ_n^i , accumulated by the sample i , placed at the distance r_i from the neutron source will be calculated as:

$$\varphi_n^i = \varphi_n^1 \cdot \frac{r_i}{r_1} \quad (3.5)$$

where φ_n^1 is the reverse fluence accumulated by the reference sample located at the distance r_1 from the neutron source.

Often, as in the present case, the two reference foils occupy the first and last positions in the assembly. For them,

$$\begin{cases} \varphi_n^1 = \varphi_0 \cdot r_1 \\ \varphi_n^2 = \varphi_0 \cdot r_2 \end{cases} \quad (3.6)$$

where φ_0 is the reverse fluence at the unitary distance from the neutron source;

r_1 and r_2 are the positions of the two reference foils.

The solution of the system (3.6) is equivalent to drawing a straight line in the plane (r, φ_n) . The straight line goes out from the point $(0, 0)$ and must pass through two other points with coordinates (r_1, φ_n^1) and (r_2, φ_n^2) . It is natural to use the method of weighted least squares for finding the slope of the line, φ_0 :

$$w_1 \cdot (\varphi_n^1 - \varphi_0 \cdot r_1)^2 + w_2 \cdot (\varphi_n^2 - \varphi_0 \cdot r_2)^2 = \min \quad (3.7)$$

where w_1 and w_2 are the weights of measurements for the first and second reference samples. Then,

$$\varphi_0 = \frac{w_1 \cdot \varphi_n^1 \cdot r_1 + w_2 \cdot \varphi_n^2 \cdot r_2}{w_1 \cdot r_1^2 + w_2 \cdot r_2^2} \quad (3.8)$$

The reverse fluence accumulated by the sample located at the distance r_i will be determined as:

$$\varphi_n^i = \varphi_0 \cdot r_i \quad (3.9)$$

It is not a rare situation when several sample packets placed at different angles to the accelerator beam are irradiated simultaneously in order to obtain cross sections at different neutron energy values. At the Khlopin Radium Institute, seven or eight packets are typically arranged near the target. To find the flux at the unitary distance, φ_0 , the same scheme can be applied to all assemblies at once. However, it is necessary to take into account two new circumstances:

- 1) the neutron source is anisotropic;

2) the effective center of the neutron beam may be shifted from the geometric center of the accelerator target.

Let us assume that there are n packets with the samples and these are placed in one plane. Then only the beam deviation in this plane will have a practical importance. Let it be denoted by u . Anisotropy of the neutron flux, $V(\vartheta)$, is defined by:

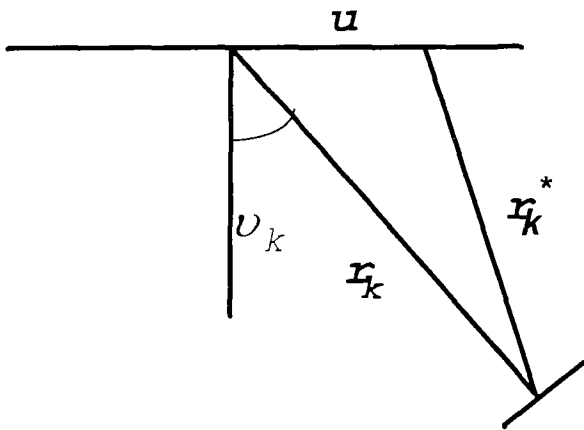
$$V(\vartheta) = \frac{\Phi(\vartheta)}{\Phi_0} \quad (3.10)$$

where $\Phi(\vartheta)$ is fluence of neutrons emitted in direction ϑ , and Φ_0 is the mean neutron fluence:

$$\Phi_0 = \frac{N_{n_tot}}{4\pi} \quad (3.11)$$

Here N_{n_tot} is the total number of neutrons emitted in all directions during the irradiation.

In Fig. 3.1 the changing of the distance to the neutron source is shown that is caused by shifting the beam center from the center of the target.



u - the deviation of the beam center from the center of the target;

r_k - the distance between the center of the target and the center of the sample;

r_k^* - the distance between the center of the sample and the effective center of the neutron beam;

ϑ_k - direction to the sample;

Fig. 3.1. The vicinity of the target.

As it is seen from Fig. 3.1, the real distance from the neutron source to the sample, r_k^* , is connected with the mechanically fixed distance from the target to the sample through:

$$r_k^{*2} = r_k^2 + u^2 + 2r_k \cdot u \cdot \sin(\vartheta_k) \quad (3.12)$$

Then we will have a system of equations like (3.7):

$$w_{1k} \cdot \left(\varphi_{1k} - \frac{\varphi_{00}}{\sqrt{V_k}} \cdot r_{1k}^* \right)^2 + w_{2k} \cdot \left(\varphi_{2k} - \frac{\varphi_{00}}{V_k} \cdot r_{2k}^* \right)^2 = \min \quad (3.13)$$

where k runs from 1 to n .

The system (3.13) has no analytical solution similar to (3.8), however it can be easily solved with a computer using an iteration procedure. As a result, the total number of neutrons emitted during the irradiation time, N_{n_tot} , and the real position of the beam on the target, u , will be deduced. It is worth noticing that for determination of these two parameters, more than two

independent equations are used. It means, the uncorrelated error of the neutron fluence determination decreases $\sqrt{n_r - 2}$ times, where n_r is the number of reference samples.

Finally, the neutron fluence accumulated by the i -sample in the k -assembly will be calculated by the formula:

$$\Phi_{ik} = \Phi_{0k} \cdot r_{ik}^* \quad (3.14)$$

$$\Phi_{0k} = \frac{1}{\sqrt{\Phi_0 \cdot V(\mathfrak{g}_k)}} \quad (3.15)$$

$$r_{ik}^{*2} = \sqrt{r_{ik}^2 + u^2 + 2r_{ik} \cdot u \cdot \sin(\varphi_k)} \quad (3.16)$$

3.3 Determination of the number of nuclei produced in the reaction

As indicated above, this analysis is restricted to activation cross section measurements. In this case, the induced activity of the sample, A_B , is measured experimentally. It is related to number of nuclei of type **B**, N_B , through the simple relation: (17)

$$A_B = \lambda_B \cdot N_B \quad (3.17)$$

where λ_B is the decay constant.

The total number of the **B** nuclei produced during the irradiation, N_{B0} , is connected with N_B by the radioactive decay law:

$$N_B = N_{B0} \cdot e^{-\lambda_B \cdot t} \quad (3.18)$$

Here t is the "age" of the sample at the moment of the measurement.

Equation (3.18) is correct if the nucleus **B** has no parent in the radioactive chain. If it has a parent nucleus **B_m** that also is produced at the irradiation, then:

$$N_B = N_{B0} \cdot e^{-\lambda_B \cdot t} \cdot \left[1 + \frac{\sigma_B}{\sigma_{B^m}} \cdot \frac{\lambda_B}{\lambda_B - \lambda_{B^m}} \cdot \left(e^{-\lambda_{B^m} \cdot t} - e^{-\lambda_B \cdot t} \right) \right] \quad (3.19)$$

The formula (3.19) covers almost all situations that have practical significance because the production of the radioactive chains consisting of three or more members is rather unusual for irradiations involving fast neutrons.

Generally speaking, the ratio $\frac{\sigma_B}{\sigma_{B^m}}$ is unknown and has to be determined from the

experimental data. Moreover, it may depend on neutron energy and, hence, is specific for each sample packet. There are some methods for its determination. At the present stage it is assumed to be deduced already. Then it is possible to take into account the influence of the finite irradiation time and fluctuation of neutron flux during the irradiation. As each group of the nuclei produced in subsequent moments of the irradiation decays independently, then:

$$N_B = N_{B0} \cdot \frac{\int_{t_1'}^{t_2'} \Phi_n(t) \cdot e^{-\lambda_B \cdot t} \cdot \left[1 + \frac{\sigma_B}{\sigma_{B^m}} \cdot \frac{\lambda_B}{\lambda_B - \lambda_{B^m}} \cdot (e^{-\lambda_{B^m} \cdot t} - e^{-\lambda_B \cdot t}) \right] \cdot dt}{\int_{t_1'}^{t_2'} \Phi_n(t) \cdot dt}, \quad (3.20)$$

where the variable t is the time between the moment of irradiation and the moment of gamma counting.

Note that this approach allows one to account for decay of reaction products during the irradiation and cooling time. The change of the induced activity during gamma counting can be accounted for in the similar way.

Since the activity averaged over the gamma counting time is obtained in the experiment

$$\overline{A_B} = \frac{\int_{t_1}^{t_2} A_B(t) \cdot dt}{t_2 - t_1}, \quad (3.21)$$

Then:

$$\overline{A_B} = \frac{N_{B0} \cdot \lambda_B}{t_2^c - t_1^c} \cdot \int_{t_1^c}^{t_2^c} dt^c \cdot \frac{\int_{t_1'}^{t_2'} \Phi_n(t) \cdot e^{-\lambda_B \cdot t} \cdot \left[1 + \frac{\sigma_B}{\sigma_{B^m}} \cdot \frac{\lambda_B}{\lambda_B - \lambda_{B^m}} \cdot (e^{-\lambda_{B^m} \cdot t} - e^{-\lambda_B \cdot t}) \right] \cdot dt}{\int_{t_1'}^{t_2'} \Phi_n(t) \cdot dt}, \quad (3.22)$$

where an additional integration is made over the counting interval (t_1^c, t_2^c) .

The mean activity can be expressed through:

$$\overline{A_B} = \frac{S_\gamma}{(t_2^c - t_1^c) \cdot \varepsilon_\gamma \cdot Y_\gamma}, \quad (3.23)$$

where S_γ is the area of the gamma-peak, ε_γ is the absolute efficiency of gamma spectrometer and Y_γ is the yield of the relevant gamma line.

At last, one has all the values that are necessary for the determination of the reaction cross section (3.1):

N_B - equations (3.17)-(3.23);

N_A - equation (3.2);

Φ_n - equations (3.3)-(3.16).

It should be noted that the algorithm described above is rather universal and includes many effects that are usually regarded as corrections. This allows to conduct the data processing in a standard way that enhances the productivity of set-up and the reliability of results. Besides, a careful calculation of geometrical factors, and detailed measurement of detector characteristics, allows to carry out experiments in "close" geometries leading to optimization of the use of the neutron flux generated by the Neutron Generator. The algorithm has been implemented in a computer code that was used for analysis of activation data measured at the Khlopin Radium Institute.

4. NEUTRON FIELD CALCULATION

A calculation of the space and energy distribution of neutrons generated in the ${}^3\text{H}(d,n){}^4\text{He}$ reaction was made taking into account the realistic experimental conditions, such as finite sizes of the beam and sample, inhomogeneity of the tritium distribution in the target, changes of the energy and angle parameters of the beam due to slowing down, etc. As the base model, the method described in [9] was used. In the present work, this approach was extended to the event of noncoaxial geometry. Some results of neutron field calculation are shown in Figs. 4.1 - 4.8.

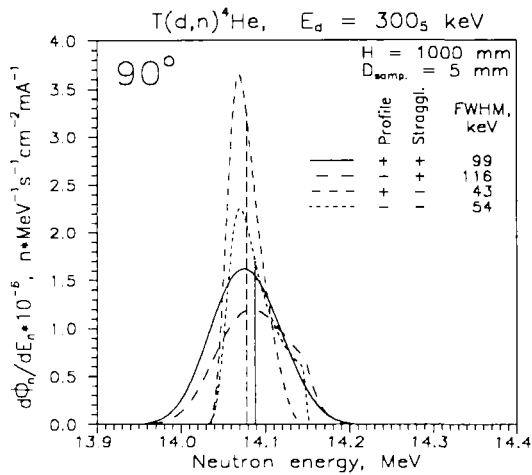


Fig. 4.1. Neutron spectra calculated by taking account (+) (or not (-)) the tritium distribution in the target and straggling effects.

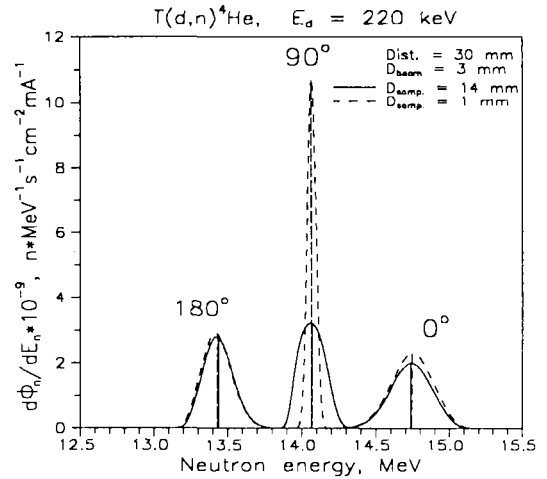


Fig. 4.3. Neutron spectra calculated for different diameters of the sample.

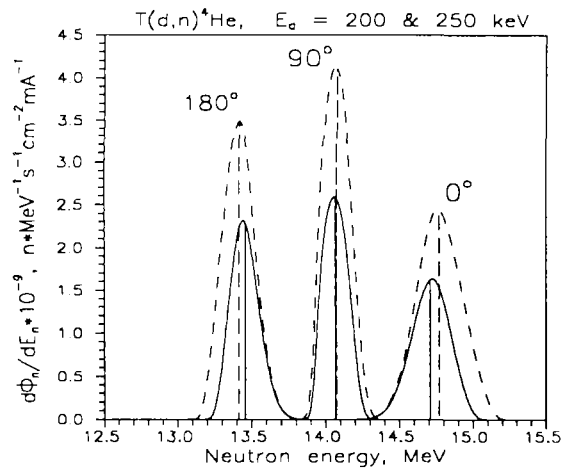


Fig. 4.2. Neutron spectra calculated for different deuteron energies

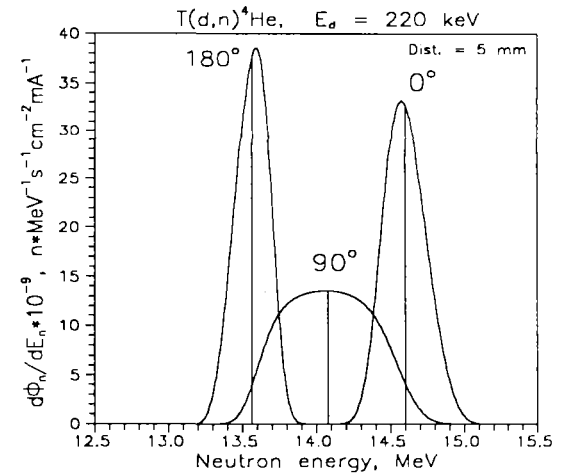


Fig. 4.4. Neutron spectra calculated for a target-sample distance of 5 mm.

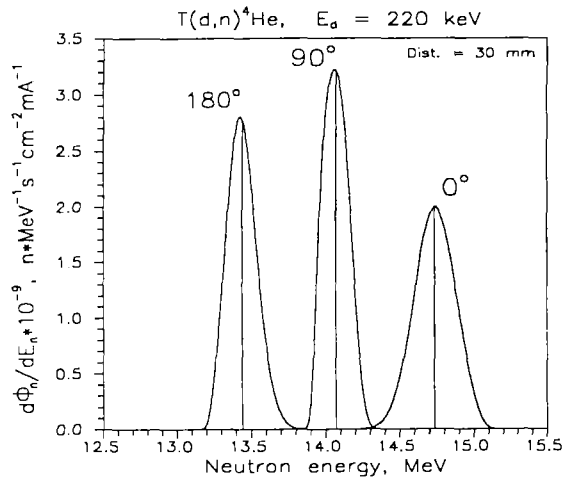


Fig. 4.5. Neutron spectra calculated for a target-sample distance of 30 mm.

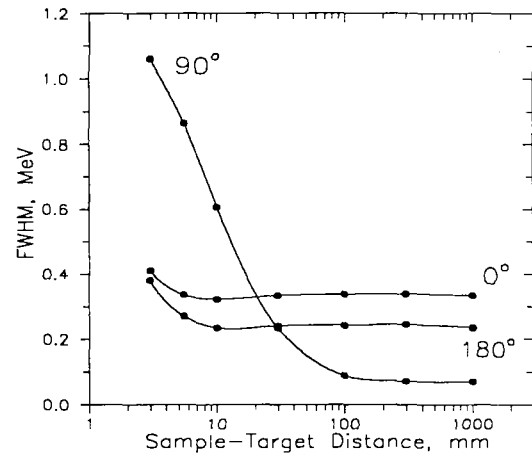


Fig. 4.7. Dependence of the full width at half of maximum (FWHM) of the neutron spectrum on the sample-target distance at $E_d = 220$ keV.

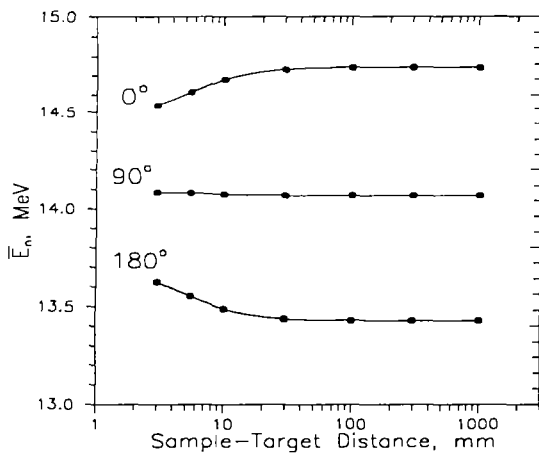


Fig. 4.6. Dependence of the averaged neutron energy on the sample-target distance at $E_d = 220$ keV.

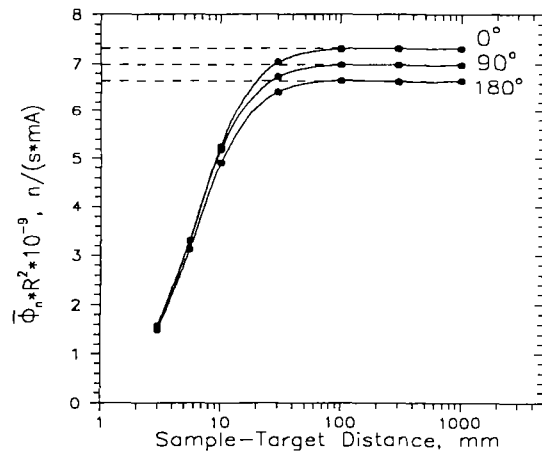


Fig. 4.8. The sample-target distance dependence of the averaged neutron flux multiplied by squared distance at $E_d = 220$ keV.

5. MAIN RESULTS OF CROSS SECTION MEASUREMENTS

The data obtained in this work are presented in Tables 5.1 - 5.70 and in Fig. 5.1 - 5.70. In these tables the cross section uncertainty is given in the absolute units. In the figures, the present data are compared only with the data of Y.Ikeda et al. [1, 2] and Zhao Wenrong et al. [3] which are, in the opinion of authors, most complete sets of experimental data obtained recently. The evaluated values of the Russian Activation Data Library ADL-3 are presented as well. This library is a most detailed library that contains more than 20000 excitation functions [10]. Sometimes, the EAF-4 evaluations are also shown in the figures.

Among the cross sections measured in this work are some that are easy to measure and are therefore known with high accuracy. These are, for example, $^{27}\text{Al}(n, p)^{27}\text{Mg}$, $^{51}\text{V}(n, \alpha)^{48}\text{Sc}$, $^{56}\text{Fe}(n, p)^{56}\text{Mn}$, $^{90}\text{Zr}(n, 2n)^{89}\text{Zr}$, etc. The present measurements were performed to confirm the correctness of the procedures used. As is seen in Figs. 5.2, 5.6, 5.9, and 5.30, in these situations the present data agree very well with evaluations and other experimental data.

The second class of measurements contains cross sections for which a definite scattering of the earlier results was observed. There is a rather large number of such cross sections. Since the possible reasons for data disagreement are various, it is impossible to discuss each reaction here due to a limitation of space. However, it is worth noticing that in most cases, but not always, the present data agree with the most recent data obtained by Y.Ikeda et al. [1, 2].

In the present work data are also presented for situations in which the data scattering was remarkable. These cross sections were recommended to be measured by IAEA specialists [11]. These are the $^{102}\text{Pd}(n, 2n)^{101}\text{Pd}$, $^{106}\text{Pd}(n, p)^{106\text{m}}\text{Rh}$ and $^{106}\text{Cd}(n, 2n)^{105}\text{Cd}$ reactions. In all the three cases, the results of the present measurements are closest to the data of reference [2]. The last reaction, the $^{106}\text{Cd}(n, 2n)^{105}\text{Cd}$ (Fig. 5.46) is most interesting because for it the data of [2] differed strongly from all others. Nevertheless, the present measurements confirmed namely these cross section values. It appears to be necessary to make the new evaluation of the $^{106}\text{Cd}(n, 2n)^{105}\text{Cd}$ cross section taking into consideration the latest experimental results.

Several cross sections were measured in the frame of Co-ordinated Research Program on Activation Cross Sections for the Generation of Long-lived Radionuclides of Importance in Fusion Reactor Technology organized by IAEA [12, 13]. From this category, the $^{109}\text{Ag}(n, 2n)^{108\text{m}}\text{Ag}$, $^{151}\text{Eu}(n, 2n)^{150\text{g}}\text{Eu}$ and $^{153}\text{Eu}(n, 2n)^{152\text{g}}\text{Eu}$ are presented in the present paper. Before the beginning of this CRP, the situation with the identified reactions was qualified as unsatisfactory. The measurements carried out in frame of CRP by several experimental groups gave the results in good agreement (Figs. 5.45, 5.64 and 5.66). This allows improvement in the accuracy of corresponding evaluations.

In this work, the results of the first measurement of the $^{241}\text{Am}(n, 2n)^{240}\text{Am}$ and $^{241}\text{Am}(n, 3n)^{239}\text{Am}$ cross sections are presented for which no experimental data were available earlier (Figs. 5.69 and 5.70). This experiment will be described in more detail in a separate paper where the yields of about 40 fission fragments will be presented as well.

Recently, some new measurements are being carried out in the Khlopin Radium Institute. Among them, the $^{50}\text{V}(n, \alpha)^{47}\text{Sc}$, $^{51}\text{V}(n, n'\alpha)^{47}\text{Sc}$, $^{50}\text{V}(n, n'\alpha)^{46}\text{Sc}$, $^{50}\text{V}(n, 2n)^{49}\text{V}$, $^{92}\text{Mo}(n, np)^{91\text{m}}\text{Mo}$, $^{92}\text{Mo}(n, np)^{91\text{g}}\text{Mo}$, $^{204}\text{Pb}(n, p)^{204}\text{Tl}$ and $^{206}\text{Pb}(n, \alpha)^{203}\text{Hg}$ reaction seem to be most interesting. Despite their importance, there is not much prior data available for them. The experiments are rather difficult but they are in progress already.

Brief information about all the reactions investigated is presented in the table 5.71. In the first column of the table the reaction is identified, the reaction energy is given in the second column, spins and parities of initial and final states are shown in the third and fourth columns. The

fifth column contains the reaction cross section at neutron energy 14.1 MeV. This cross section was obtained by approximating the experimental data by the straight line whose parameters were calculated by the weighed mean squares method. In the sixth column, the cross section rate of change averaged over the energy interval covered is given.

Tables 5.1-5.70 Cross section data measured.

5.1. $^{23}\text{Na}(n, 2n)^{22}\text{Na}$

E_n , (MeV)	Cross Section, (mb)
13.56	4.58 (0.97)
13.74	9.79 (0.98)
13.96	14.0 (0.11)
14.19	21.9 (0.15)
14.42	29.9 (0.19)
14.61	32.4 (0.17)
14.78	37.6 (0.17)

5.5. $^{41}\text{K}(n, p)^{41}\text{Ar}$

E_n , (MeV)	Cross Section, (mb)
13.48	55.3 (2.5)
13.65	55.9 (2.4)
13.87	51.4 (2.5)
14.07	53.5 (2.4)
14.27	50.3 (2.2)
14.46	49.1 (2.1)
14.66	49.8 (2.0)
14.85	46.6 (2.0)

5.2. $^{27}\text{Al}(n, p)^{27}\text{Mg}$

E_n , (MeV)	Cross Section, (mb)
13.47	78.4 (1.7)
13.66	72.9 (1.6)
13.88	74.7 (1.6)
14.04	70.6 (1.6)
14.26	69.9 (1.5)
14.44	70.3 (1.5)
14.63	65.3 (1.5)
14.81	62.9 (1.4)

5.6. $^{51}\text{V}(n, \alpha)^{48}\text{Sc}$

E_n , (MeV)	Cross Section, (mb)
13.56	14.51 (0.45)
13.74	15.02 (0.55)
13.96	14.98 (0.57)
14.19	16.56 (0.54)
14.42	16.92 (0.56)
14.61	17.53 (0.65)
14.78	18.25 (0.60)

5.3. $^{39}\text{K}(n, 2n)^{38}\text{K}$

E_n , (MeV)	Cross Section, (mb)
13.48	0.034 (0.015)
13.65	0.24 (0.03)
13.87	0.68 (0.04)
14.07	1.39 (0.15)
14.27	2.50 (0.13)
14.46	3.08 (0.16)
14.66	4.52 (0.25)
14.85	5.37 (0.30)

5.7. $^{55}\text{Mn}(n, \alpha)^{52}\text{V}$

E_n , (MeV)	Cross Section, (mb)
13.47	20.6 (0.8)
13.66	20.9 (0.9)
13.88	22.6 (1.0)
14.04	22.7 (1.0)
14.26	22.9 (1.0)
14.44	23.3 (0.9)
14.63	23.5 (0.9)
14.81	22.8 (1.0)

5.4. $^{41}\text{K}(n, \alpha)^{38}\text{Cl}$

E_n , (MeV)	Cross Section, (mb)
13.48	39.2 (2.3)
13.65	36.4 (2.2)
13.87	35.2 (2.0)
14.07	35.7 (1.9)
14.27	33.6 (1.9)
14.46	34.0 (2.0)
14.66	30.4 (1.9)
14.85	30.8 (1.8)

5.8. $^{55}\text{Mn}(n, 2n)^{54}\text{Mn}$

E_n , (MeV)	Cross Section, (mb)
13.56	620 (26)
13.74	632 (26)
13.96	656 (27)
14.19	708 (27)
14.42	740 (28)
14.61	763 (27)
14.78	781 (28)

5.9. $^{56}\text{Fe}(n, p)^{56}\text{Mn}$

E_n (MeV)	Cross Section, (mb)
13.56	115.3 (4.2)
13.74	115.3 (4.3)
13.96	111.8 (2.3)
14.19	113.7 (2.4)
14.42	109.0 (2.6)
14.61	105.8 (2.3)
14.78	103.9 (2.1)

5.10. $^{59}\text{Co}(n, \alpha)^{56}\text{Mn}$

E_n (MeV)	Cross Section, (mb)
13.56	31.27 (0.97)
13.74	31.04 (0.78)
13.96	31.70 (0.98)
14.19	31.47 (0.82)
14.42	31.89 (0.78)
14.61	31.48 (0.79)
14.78	32.09 (0.83)

5.11. $^{59}\text{Co}(n, p)^{59}\text{Fe}$

E_n (MeV)	Cross Section, (mb)
13.56	53.0 (1.9)
13.74	52.5 (1.9)
13.96	51.0 (1.8)
14.19	51.6 (1.9)
14.42	47.8 (1.7)
14.61	46.2 (1.6)
14.78	47.18 (1.6)

5.12. $^{59}\text{Co}(n, 2n)^{58m}\text{Co}$

E_n (MeV)	Cross Section, (mb)
13.56	384 (14)
13.74	410 (14)
13.96	401 (23)
14.19	439 (18)
14.42	478 (17)
14.61	481 (19)
14.78	482 (18)

5.13. $^{59}\text{Co}(n, 2n)^{58m+g}\text{Co}$

E_n (MeV)	Cross Section, (mb)
13.56	588 (21)
13.74	627 (21)
13.96	658 (25)
14.19	668 (25)
14.42	728 (25)
14.61	731 (27)
14.78	731 (26)

5.14. $^{58}\text{Ni}(n, np)^{57}\text{Co}$

E_n (MeV)	Cross Section, (mb)
13.47	511 (29)
13.56	538 (27)
13.64	548 (22)
13.74	570 (16)
13.88	561 (32)
13.96	589 (18)
14.05	597 (26)
14.19	637 (19)
14.28	637 (27)
14.42	656 (33)
14.47	650 (32)
14.61	676 (21)
14.68	658 (34)
14.78	679 (28)
14.86	682 (28)

5.15. $^{58}\text{Ni}(n, p)^{58m}\text{Co}$

E_n (MeV)	Cross Section, (mb)
13.56	234 (9)
13.74	218 (9)
13.96	197 (8)
14.19	182 (8)
14.42	170 (7)
14.61	173 (11)
14.78	150 (6)

5.16. $^{58}\text{Ni}(n, p)^{58m+g}\text{Co}$

E_n (MeV)	Cross Section, (mb)
13.47	421 (28)
13.56	414 (14)
13.64	394 (20)
13.74	383 (16)
13.88	374 (25)
13.96	359 (17)
14.05	351 (18)
14.19	330 (14)
14.28	339 (20)
14.42	314 (14)
14.47	315 (16)
14.61	292 (14)
14.68	293 (18)
14.78	276 (12)
14.86	273 (17)

5.17. $^{58}\text{Ni}(n, 2n)^{57}\text{Ni}$

E_n (MeV)	Cross Section. (mb)
13.47	11.52 (0.37)
13.56	12.55 (0.46)
13.64	14.55 (0.40)
13.74	15.29 (0.52)
13.88	19.55 (0.59)
13.96	20.01 (0.62)
14.05	23.42 (0.65)
14.19	25.04 (1.31)
14.28	27.73 (0.95)
14.42	29.76 (1.10)
14.47	32.92 (0.83)
14.61	33.38 (0.68)
14.68	35.90 (1.00)
14.78	35.68 (0.75)
14.86	39.07 (1.01)

5.18. $^{60}\text{Ni}(n, p)^{60}\text{Co}$

E_n (MeV)	Cross Section. (mb)
13.47	166.7 (5.9)
13.64	158.8 (6.6)
13.88	156.8 (4.9)
14.05	157.4 (4.6)
14.28	155.1 (4.6)
14.44	150.7 (6.3)
14.63	142.6 (7.1)
14.86	136.7 (6.4)

5.19. $^{63}\text{Cu}(n, \alpha)^{60}\text{Co}$

E_n (MeV)	Cross Section. (mb)
13.47	47.5 (2.7)
13.64	45.6 (1.6)
13.88	45.6 (2.5)
14.05	45.5 (1.4)
14.28	45.8 (1.4)
14.44	46.1 (1.7)
14.63	43.2 (1.5)
14.86	42.3 (1.3)

5.20. $^{65}\text{Cu}(n, p)^{65}\text{Ni}$

E_n (MeV)	Cross Section. (mb)
13.56	22.33 (0.76)
13.74	20.28 (1.27)
13.96	21.45 (0.91)
14.19	20.45 (1.16)
14.42	20.36 (0.71)
14.61	21.46 (0.65)
14.78	20.58 (0.87)

5.21. $^{65}\text{Cu}(n, 2n)^{64}\text{Cu}$

E_n (MeV)	Cross Section. (mb)
13.56	834 (49)
13.74	863 (37)
13.96	918 (62)
14.19	867 (37)
14.42	952 (43)
14.61	903 (38)
14.78	965 (50)

5.22. $^{88}\text{Sr}(n, \alpha)^{85\text{m}}\text{Kr}$

E_n (MeV)	Cross Section. (mb)
13.47	0.80 (0.08)
13.64	1.03 (0.09)
13.88	1.06 (0.08)
14.05	1.24 (0.09)
14.28	1.30 (0.10)
14.47	1.36 (0.10)
14.68	1.51 (0.11)
14.86	1.61 (0.10)

5.23. $^{88}\text{Sr}(n, 2n)^{87\text{m}}\text{Sr}$

E_n (MeV)	Cross Section. (mb)
13.47	175 (11)
13.64	197 (11)
13.88	215 (13)
14.05	227 (12)
14.28	242 (12)
14.47	248 (12)
14.68	269 (17)
14.86	280 (14)

5.24. $^{89}\text{Y}(n, \alpha)^{86\text{m}}\text{Rb}$

E_n (MeV)	Cross Section. (mb)
13.47	1.03 (0.26)
13.65	1.19 (0.17)
13.88	1.3 (0.19)
14.04	1.32 (0.19)
14.26	1.6 (0.30)
14.43	1.81 (0.16)
14.62	1.84 (0.18)
14.78	1.99 (0.19)

5.25. $^{89}\text{Y}(n, \alpha)^{86\text{m}+g}\text{Rb}$

E_n (MeV)	Cross Section. (mb)
13.47	4.41 (0.76)
13.65	5.81 (0.96)
13.88	5.64 (1.00)
14.04	5.56 (1.00)
14.28	6.56 (1.20)
14.47	6.24 (1.20)
14.68	7.32 (1.10)
14.86	7.35 (1.20)

5.26. $^{89}\text{Y}(n, 2n)^{88}\text{Y}$

E_n (MeV)	Cross Section. (mb)
13.47	680 (21)
13.64	725 (23)
13.88	791 (26)
14.05	887 (29)
14.28	902 (28)
14.47	961 (28)
14.68	978 (30)
14.86	1031 (30)

5.31. $^{92}\text{Zr}(n, p)^{92}\text{Y}$

E_n (MeV)	Cross Section. (mb)
13.56	14.2 (2.0)
13.74	16.4 (2.1)
13.96	19.6 (2.3)
14.19	18.7 (2.1)
14.42	19.6 (2.1)
14.61	22.9 (2.4)
14.78	20.5 (2.3)

5.27. $^{90}\text{Zr}(n, \alpha)^{87\text{m}}\text{Sr}$

E_n (MeV)	Cross Section. (mb)
13.56	3.50 (0.30)
13.74	3.51 (0.27)
13.96	3.70 (0.21)
14.19	4.00 (0.28)
14.42	4.07 (0.27)
14.61	4.00 (0.41)
14.78	4.09 (0.23)

5.32. $^{94}\text{Zr}(n, \alpha)^{91}\text{Sr}$

E_n (MeV)	Cross Section. (mb)
13.56	4.20 (0.49)
13.74	4.51 (0.43)
13.96	4.74 (0.34)
14.19	4.62 (0.45)
14.42	4.90 (0.43)
14.61	5.00 (0.49)
14.78	5.30 (0.36)

5.28. $^{90}\text{Zr}(n, p)^{90\text{m}}\text{Y}$

E_n (MeV)	Cross Section. (mb)
13.56	10.86 (0.47)
13.74	11.36 (0.50)
13.96	11.89 (0.48)
14.19	12.07 (0.59)
14.42	12.50 (0.56)
14.61	12.25 (0.40)
14.78	12.44 (0.44)

5.33. $^{96}\text{Zr}(n, 2n)^{95}\text{Zr}$

E_n (MeV)	Cross Section. (mb)
13.56	1621 (106)
13.74	1600 (153)
13.96	1580 (78)
14.19	1538 (65)
14.42	1627 (149)
14.61	1624 (165)
14.78	1607 (88)

5.29. $^{90}\text{Zr}(n, 2n)^{89\text{m}}\text{Zr}$

E_n (MeV)	Cross Section. (mb)
13.47	30.82 (0.81)
13.66	40.11 (1.23)
13.88	62.8 (1.6)
14.04	77.8 (2.1)
14.26	92.5 (2.7)
14.44	116.3 (2.9)
14.63	124.2 (3.2)
14.81	142.0 (3.6)

5.34. $^{93}\text{Nb}(n, \alpha)^{90\text{m}}\text{Y}$

E_n (MeV)	Cross Section. (mb)
13.47	5.12 (0.54)
13.56	4.87 (0.33)
13.64	5.17 (0.37)
13.74	5.20 (0.28)
13.88	5.33 (0.26)
13.96	5.40 (0.33)
14.05	5.75 (0.27)
14.19	5.77 (0.31)
14.28	5.66 (0.24)
14.42	5.68 (0.22)
14.47	5.95 (0.27)
14.61	5.90 (0.32)
14.68	5.82 (0.33)
14.78	5.87 (0.36)
14.86	5.97 (0.34)

5.30. $^{90}\text{Zr}(n, 2n)^{89\text{m}+g}\text{Zr}$

E_n (MeV)	Cross Section. (mb)
13.56	447 (10)
13.74	497 (10)
13.96	577 (12)
14.19	639 (13)
14.42	704 (15)
14.61	740 (16)
14.78	774 (16)

5.35. $^{93}\text{Nb}(n, 2n)^{92m}\text{Nb}$

E_n (MeV)	Cross Section, (mb)
13.47	451.7 (6.2)
13.56	452.4 (5.7)
13.64	452.4 (6.2)
13.74	453.6 (5.6)
13.88	454.9 (6.2)
13.96	455.6 (5.6)
14.05	457.1 (6.5)
14.19	459.1 (5.6)
14.28	459.2 (6.7)
14.42	460.2 (5.6)
14.47	460.4 (6.6)
14.61	459.9 (5.6)
14.68	458.9 (6.7)
14.78	457.3 (5.5)
14.86	455.3 (6.2)

5.36. $^{92}\text{Mo}(n, \alpha)^{89m}\text{Zr}$

E_n (MeV)	Cross Section, (mb)
13.47	6.42 (0.27)
13.66	6.10 (0.39)
13.88	6.67 (0.31)
14.04	6.60 (0.40)
14.26	6.53 (0.42)
14.44	7.16 (0.59)
14.63	6.82 (0.30)
14.81	6.73 (0.56)

5.37. $^{92}\text{Mo}(n, \alpha)^{89m+g}\text{Zr}$

E_n (MeV)	Cross Section, (mb)
13.47	21.1 (1.3)
13.66	20.6 (1.2)
13.88	21.3 (1.5)
14.04	24.6 (2.3)
14.26	22.9 (0.9)
14.44	24.3 (1.7)
14.63	24.4 (0.9)
14.81	26.5 (1.4)

5.38. $^{92}\text{Mo}(n, p)^{92m}\text{Nb}$

E_n (MeV)	Cross Section, (mb)
13.47	79.4 (3.2)
13.66	77.3 (5.0)
13.88	72.8 (2.5)
14.04	74.4 (3.3)
14.26	66.7 (4.4)
14.44	64.9 (2.4)
14.63	60.8 (2.7)
14.81	60.0 (2.1)

5.39. $^{92}\text{Mo}(n, 2n)^{91m}\text{Mo}$

E_n (MeV)	Cross Section, (mb)
13.66	1.44 (0.60)
13.88	3.68 (0.60)
14.04	6.43 (0.80)
14.26	11.0 (1.3)
14.44	16.2 (2.2)
14.64	22.4 (2.8)
14.81	26.9 (3.2)

5.40. $^{102}\text{Pd}(n, 2n)^{101}\text{Pd}$

E_n (MeV)	Cross Section, (mb)
13.47	840.1 (43)
13.64	861.4 (45)
13.88	914.8 (47)
14.05	985.7 (52)
14.28	1023.6 (54)
14.47	1035.7 (53)
14.68	1030.2 (55)
14.86	1049.1 (55)

5.41. $^{106}\text{Pd}(n, \alpha)^{103}\text{Ru}$

E_n (MeV)	Cross Section, (mb)
13.47	3.3 (0.5)
13.64	4.6 (0.6)
13.88	4.8 (0.8)
14.05	4.9 (0.6)
14.28	4.9 (0.6)
14.47	4.9 (0.5)
14.68	5.4 (0.5)
14.86	5.6 (0.7)

5.42. $^{106}\text{Pd}(n, p)^{106m}\text{Rh}$

E_n (MeV)	Cross Section, (mb)
13.47	6.71 (0.49)
13.64	6.91 (0.48)
13.88	7.98 (0.54)
14.05	7.97 (0.54)
14.28	8.08 (0.55)
14.42	9.07 (0.61)
14.61	9.42 (0.65)
14.78	9.67 (0.68)

5.43. $^{108}\text{Pd}(n, \alpha)^{105}\text{Ru}$

E_n (MeV)	Cross Section, (mb)
13.47	2.17 (0.25)
13.64	2.35 (0.31)
13.88	2.38 (0.32)
14.05	2.69 (0.31)
14.28	2.87 (0.38)
14.47	3.26 (0.32)
14.68	3.25 (0.31)
14.86	3.70 (0.48)

5.44. $^{107}\text{Ag}(n, 2n)^{106m}\text{Ag}$

E_n (MeV)	Cross Section, (mb)
13.74	541 (19)
13.96	577 (20)
14.19	601 (21)
14.42	592 (21)
14.61	599 (21)
14.78	599 (20)

5.45. $^{109}\text{Ag}(n, 2n)^{108m}\text{Ag}$

E_n (MeV)	Cross Section, (mb)
13.70	634 (40)
14.10	682 (40)
14.50	695 (40)
14.80	709 (40)

5.46. $^{106}\text{Cd}(n, 2n)^{105}\text{Cd}$

E_n (MeV)	Cross Section, (mb)
13.47	398 (37)
13.64	439 (44)
13.88	454 (42)
14.05	482 (40)
14.28	477 (48)
14.47	546 (54)
14.68	521 (41)
14.86	555 (58)

5.47. $^{112}\text{Cd}(n, p)^{112}\text{Ag}$

E_n (MeV)	Cross Section, (mb)
13.47	10.1 (1.0)
13.64	10.4 (1.0)
13.88	12.1 (1.1)
14.05	13.5 (1.3)
14.28	14.7 (1.2)
14.47	14.6 (1.2)
14.68	16.9 (1.3)
14.86	15.3 (1.2)

5.48. $^{112}\text{Cd}(n, 2n)^{111m}\text{Cd}$

E_n (MeV)	Cross Section, (mb)
13.47	642 (52)
13.64	625 (59)
13.88	634 (52)
14.05	627 (50)
14.28	592 (59)
14.47	635 (52)
14.68	647 (49)
14.86	643 (44)

5.49. $^{116}\text{Cd}(n, 2n)^{115g}\text{Cd}$

E_n (MeV)	Cross Section, (mb)
13.56	851 (27)
13.74	834 (25)
13.96	825 (45)
14.19	830 (26)
14.42	815 (26)
14.61	802 (54)
14.78	806 (56)

5.50. $^{113}\text{In}(n, n')^{113m}\text{In}$

E_n (MeV)	Cross Section, (mb)
13.56	73.6 (5.0)
13.74	60.5 (5.0)
13.96	68.0 (5.9)
14.19	59.2 (4.7)
14.42	52.6 (5.4)
14.61	54.2 (6.2)
14.78	51.8 (5.8)

5.51. $^{115}\text{In}(n, \alpha)^{112}\text{Ag}$

E_n (MeV)	Cross Section, (mb)
13.56	1.66 (0.18)
13.74	1.92 (0.22)
13.96	2.03 (0.18)
14.19	2.30 (0.20)
14.42	2.05 (0.16)
14.61	2.26 (0.18)
14.78	2.58 (0.20)

5.52. $^{115}\text{In}(n, p)^{115m}\text{Cd}$

E_n (MeV)	Cross Section, (mb)
13.47	3.99 (0.86)
13.64	4.08 (0.79)
13.88	4.84 (0.83)
14.05	5.04 (0.85)
14.28	5.15 (0.86)
14.47	5.20 (0.88)
14.68	5.60 (0.90)
14.86	6.09 (0.96)

5.53. $^{115}\text{In}(n, p)^{115g}\text{Cd}$.

E_n (MeV)	Cross Section, (mb)
13.47	3.90 (0.38)
13.64	3.81 (0.20)
13.88	4.30 (0.19)
14.05	4.62 (0.41)
14.28	4.78 (0.32)
14.47	4.94 (0.20)
14.68	4.97 (0.20)
14.86	5.15 (0.19)

5.54. $^{115}\text{In}(n, 2n)^{114m}\text{In}$

E_n (MeV)	Cross Section, (mb)
13.56	1228 (71)
13.74	1242 (100)
13.96	1328 (65)
14.19	1331 (120)
14.42	1314 (68)
14.61	1426 (100)
14.78	1249 (85)

5.55. $^{115}\text{In}(n, n')^{115m}\text{In}$

E_n (MeV)	Cross Section, (mb)
13.56	79.3 (4.4)
13.74	72.0 (4.2)
13.96	67.4 (3.2)
14.19	64.5 (3.9)
14.42	61.9 (3.1)
14.61	62.0 (3.1)
14.78	59.0 (3.0)

5.56. $^{138}\text{Ba}(n, \alpha)^{135m}\text{Xe}$

E_n (MeV)	Cross Section, (mb)
13.47	0.73 (0.06)
13.66	0.72 (0.07)
13.88	0.86 (0.06)
14.04	0.79 (0.07)
14.26	0.98 (0.07)
14.44	0.98 (0.06)
14.63	0.98 (0.06)
14.81	1.11 (0.06)

5.57. $^{138}\text{Ba}(n, \alpha)^{135m+g}\text{Xe}$

E_n (MeV)	Cross Section, (mb)
13.47	1.86 (0.11)
13.66	2.05 (0.13)
13.88	2.27 (0.15)
14.04	2.21 (0.15)
14.26	2.40 (0.15)
14.44	2.63 (0.17)
14.63	2.55 (0.17)
14.81	2.71 (0.17)

5.58. $^{138}\text{Ba}(n, x)^{137}\text{Cs}$

E_n (MeV)	Cross Section, (mb)
13.73	0.36 (0.07)
14.73	1.21 (0.14)

5.59. $^{138}\text{Ba}(n, p)^{138}\text{Cs}$

E_n (MeV)	Cross Section, (mb)
13.47	1.60 (0.12)
13.66	1.76 (0.12)
13.88	2.09 (0.14)
14.04	2.14 (0.14)
14.26	2.27 (0.13)
14.44	2.60 (0.14)
14.63	2.74 (0.14)
14.81	2.92 (0.16)

5.60. $^{138}\text{Ba}(n, 2n)^{137m}\text{Ba}$

E_n (MeV)	Cross Section, (mb)
13.47	796 (31)
13.64	771 (30)
13.88	800 (35)
14.05	818 (34)
14.28	834 (43)
14.47	886 (33)
14.68	874 (34)
14.81	897 (36)
14.86	939 (35)

5.61. $^{151}\text{Eu}(n, \alpha)^{148m}\text{Pm}$

E_n (MeV)	Cross Section, (mb)
13.56	1.82 (0.29)
13.74	2.13 (0.26)
13.96	1.89 (0.23)
14.19	2.19 (0.24)
14.42	1.98 (0.23)
14.61	2.41 (0.36)
14.78	2.01 (0.20)

5.62. $^{151}\text{Eu}(n, 3n)^{149}\text{Eu}$

E_n (MeV)	Cross Section, (mb)
14.65	0.2 (0.2)
14.81	1.26 (0.24)

5.63. $^{151}\text{Eu}(n, 2n)^{150m}\text{Eu}$

E_n (MeV)	Cross Section, (mb)
13.56	500 (100)
13.74	498 (98)
13.96	498 (96)
14.19	504 (102)
14.42	520 (110)
14.61	496 (98)
14.78	506 (105)

5.64. $^{151}\text{Eu}(n, 2n)^{150g}\text{Eu}$

E_n (MeV)	Cross Section, (mb)
13.56	1127 (63)
13.74	1167 (60)
13.96	1137 (63)
14.19	1091 (64)
14.42	1126 (57)
14.61	1140 (55)
14.78	1218 (54)

5.65. $^{153}\text{Eu}(n, 2n)^{152m1}\text{Eu}$

E_n (MeV)	Cross Section, (mb)
13.56	292 (42)
13.74	286 (39)
13.96	282 (39)
14.19	285 (40)
14.42	281 (39)
14.61	275 (40)
14.78	266 (39)

5.66. $^{153}\text{Eu}(n, 2n)^{152m2+g}\text{Eu}$

E_n (MeV)	Cross Section, (mb)
13.56	1464 (70)
13.74	1515 (74)
13.96	1516 (67)
14.19	1500 (76)
14.42	1445 (68)
14.61	1545 (63)
14.78	1460 (58)

5.67. $^{204}\text{Pb}(n, 2n)^{203}\text{Pb}$

E_n (MeV)	Cross Section, (mb)
13.47	2044 (162)
13.64	2179 (176)
13.88	2158 (169)
14.05	2134 (182)
14.28	2203 (177)
14.47	2164 (175)
14.68	2216 (191)
14.86	2185 (183)

5.68. $^{238}\text{U}(n, 2n)^{237}\text{U}$

E_n (MeV)	Cross Section, (mb)
13.47	692 (52)
13.64	752 (64)
13.88	786 (59)
14.05	858 (63)
14.28	959 (76)
14.47	1048 (78)
14.68	1105 (82)
14.86	1204 (101)

5.69. $^{241}\text{Am}(n, 2n)^{240}\text{Am}$

E_n (MeV)	Cross Section, (mb)
13.42	253 (24)
13.48	247 (20)
13.56	239 (25)
14.09	207 (22)
14.21	229 (25)
14.69	199 (22)
14.84	193 (22)
14.86	215(15)

5.70. $^{241}\text{Am}(n, 3n)^{241}\text{Am}$

E_n (MeV)	Cross Section, (mb)
14.73	3 (2)
14.86	12 (3)

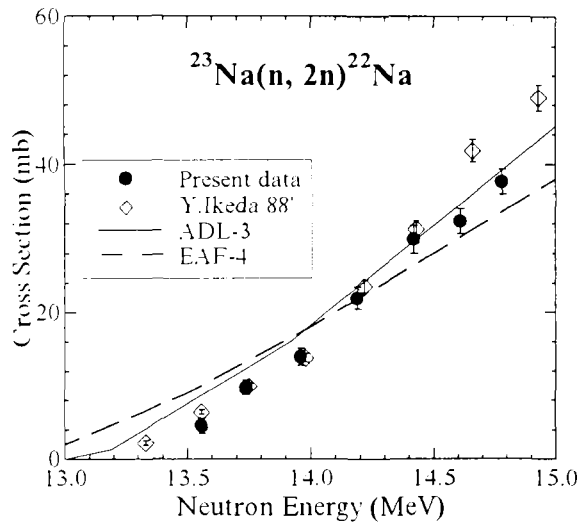


Fig. 5.1.

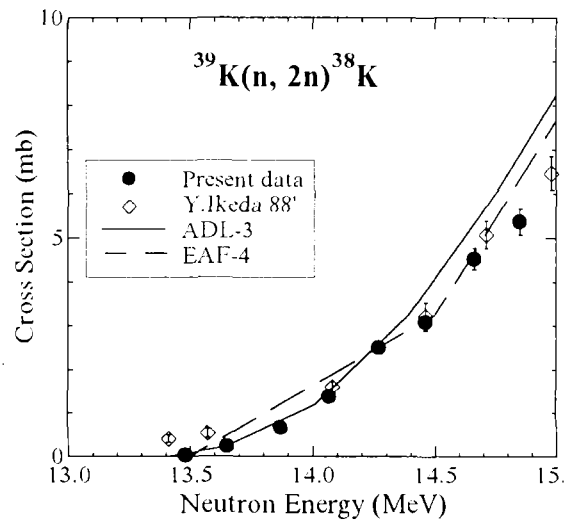


Fig. 5.4.

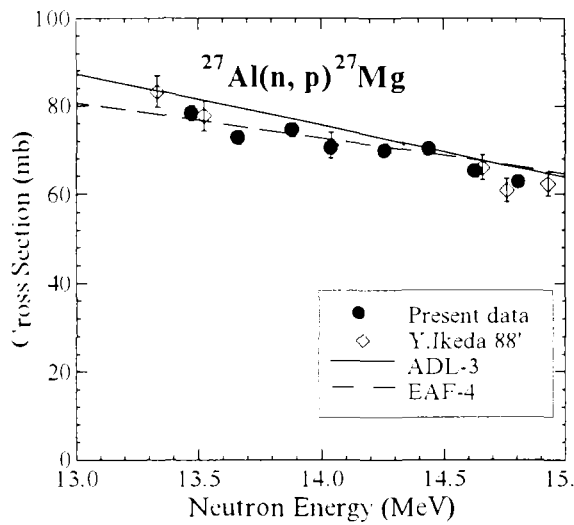


Fig. 5.2.

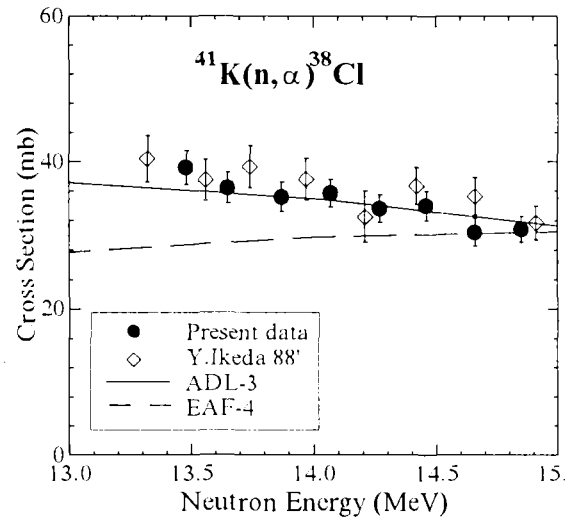


Fig. 5.5.

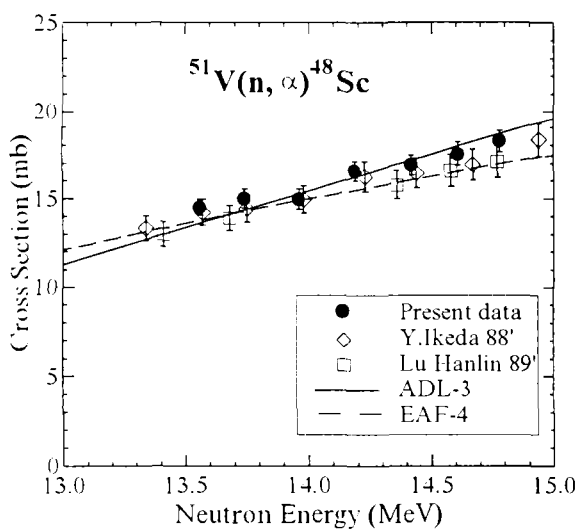


Fig. 5.3.

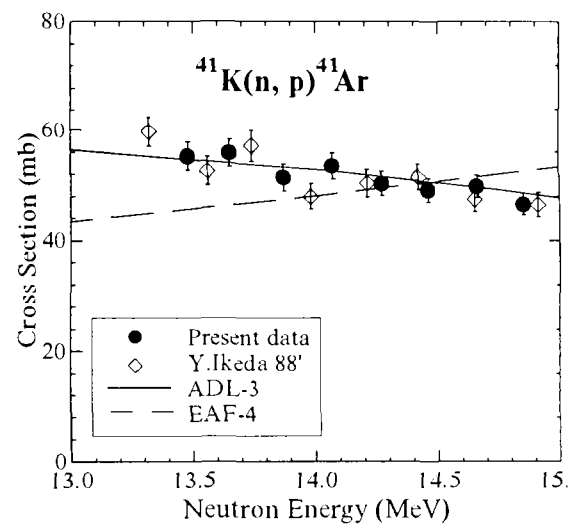


Fig. 5.6.

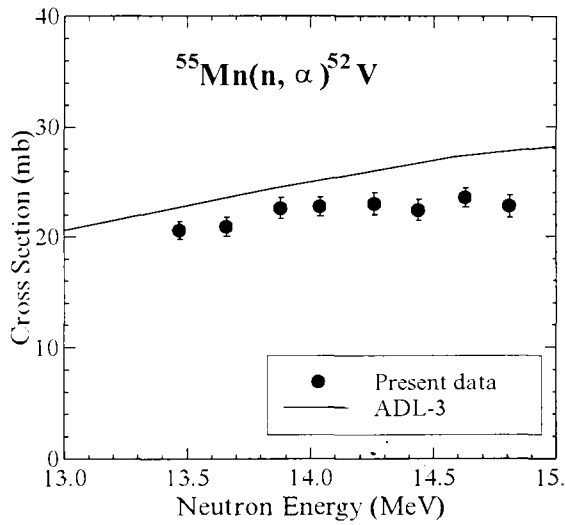


Fig. 5.7.

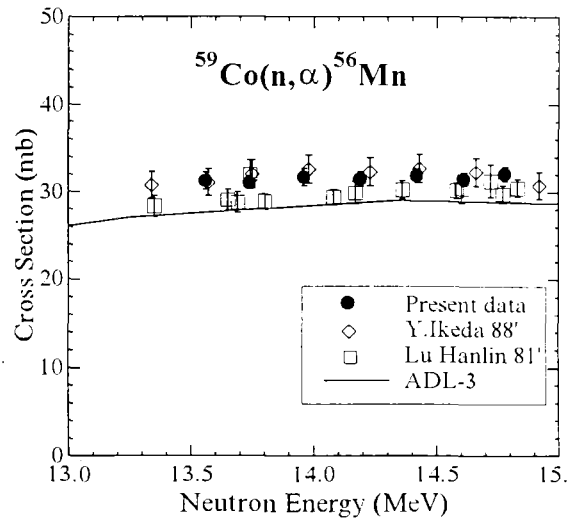


Fig. 5.10.

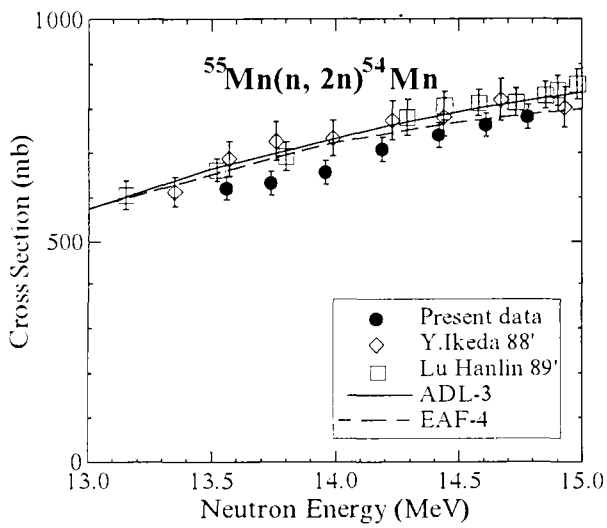


Fig. 5.8.

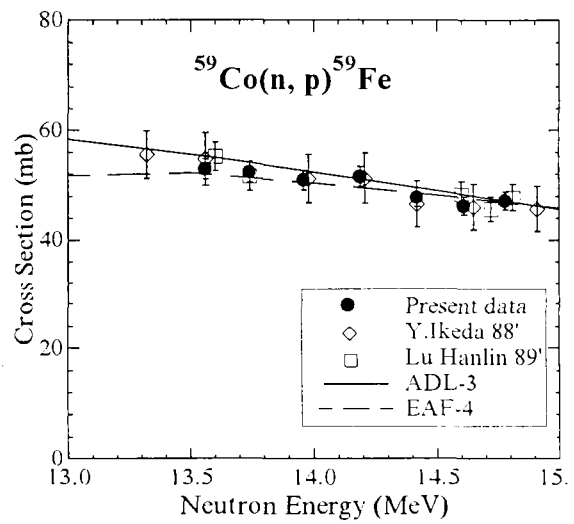


Fig. 5.11.

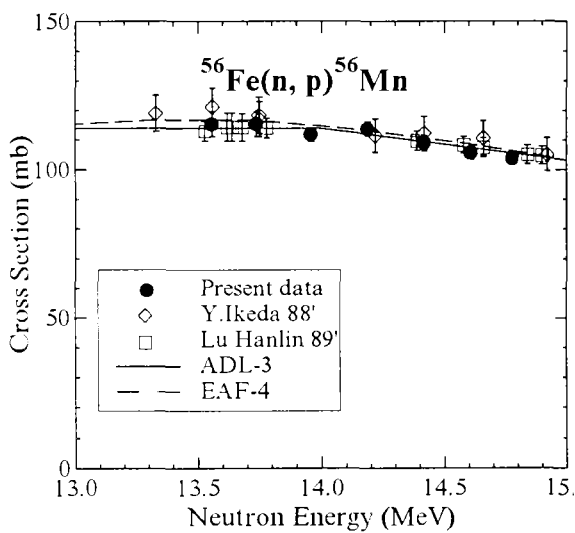


Fig. 5.9.

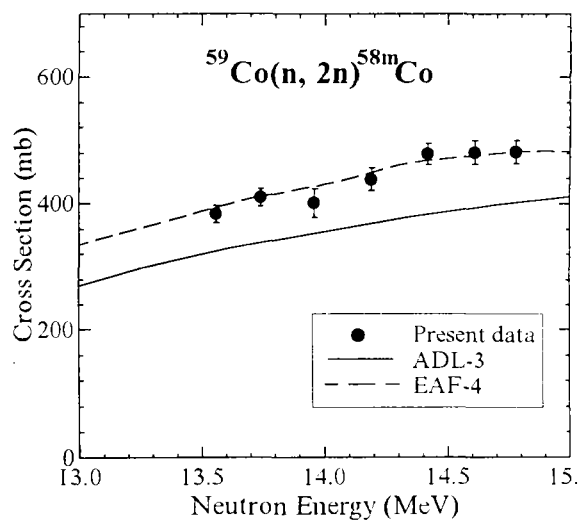


Fig. 5.12.

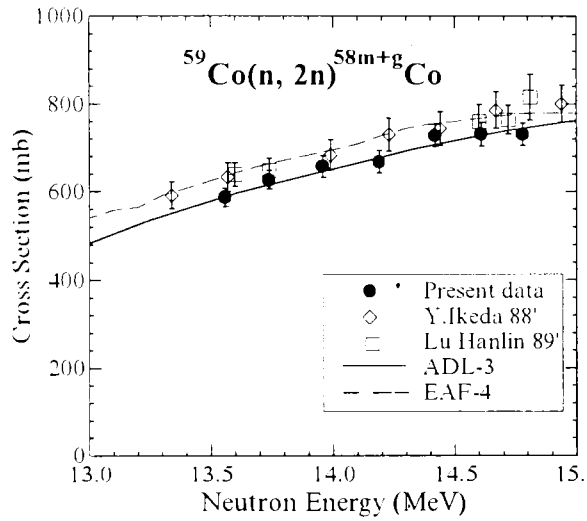


Fig. 5.13.

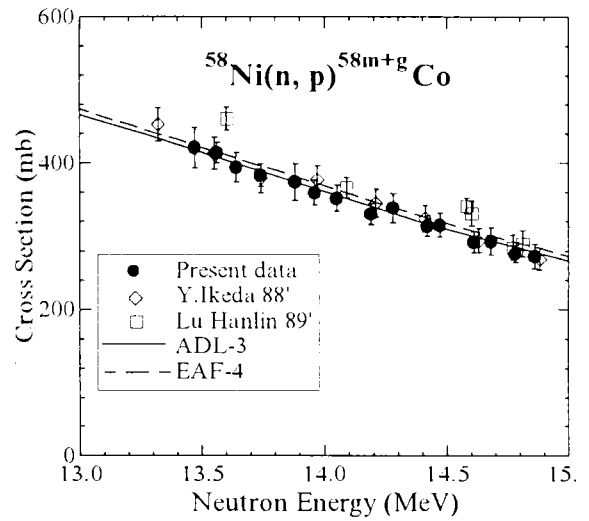


Fig. 5.16.

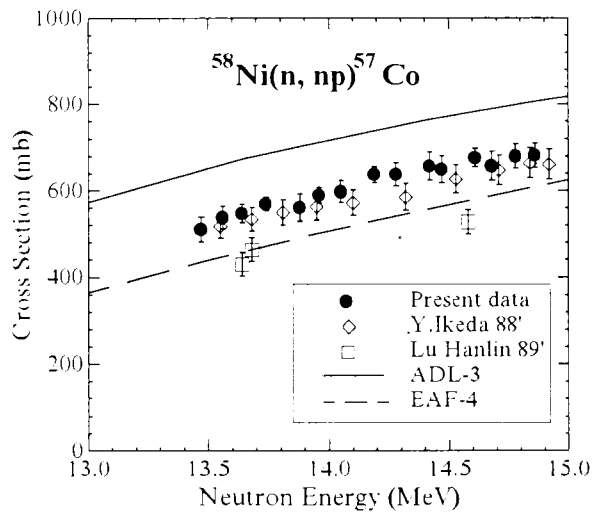


Fig. 5.14.

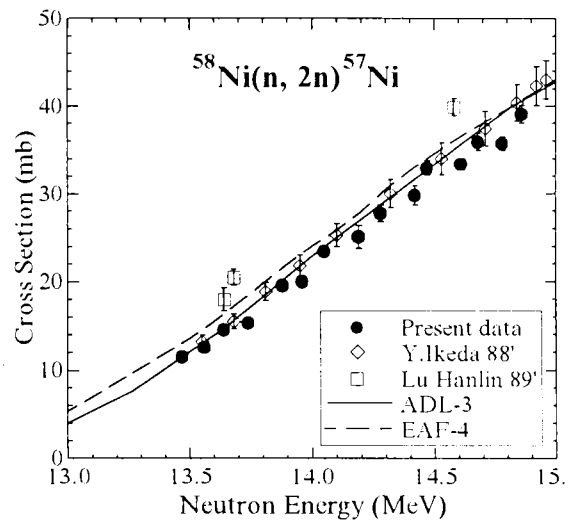


Fig. 5.17.

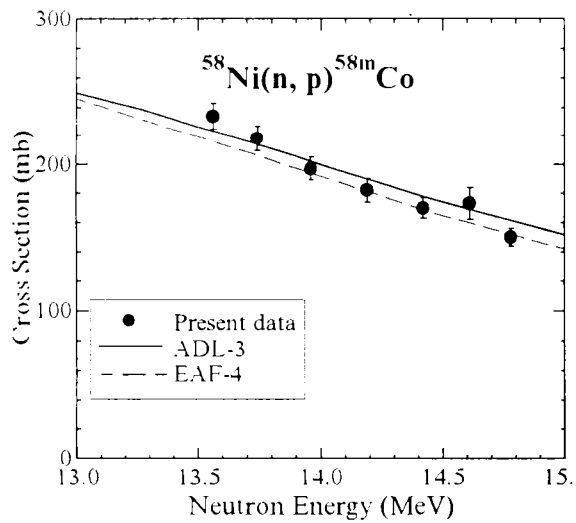


Fig. 5.15.

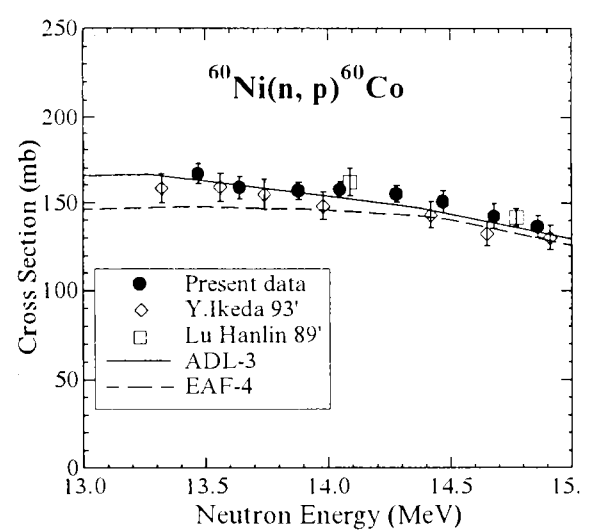


Fig. 5.18.

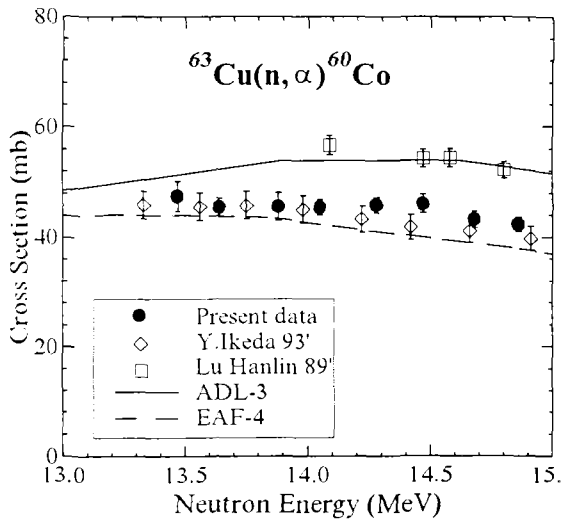


Fig. 5.19.

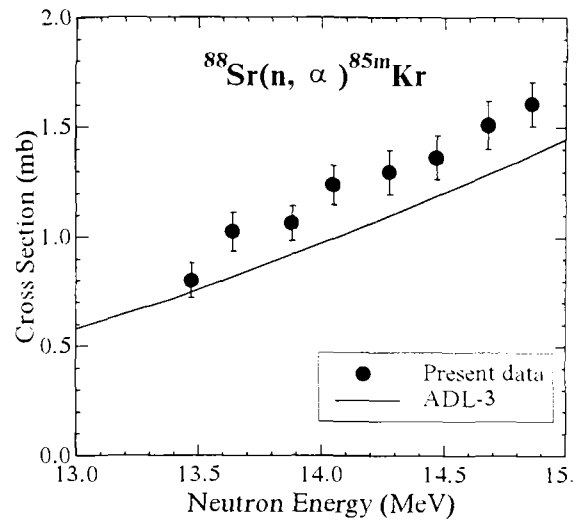


Fig. 5.22.

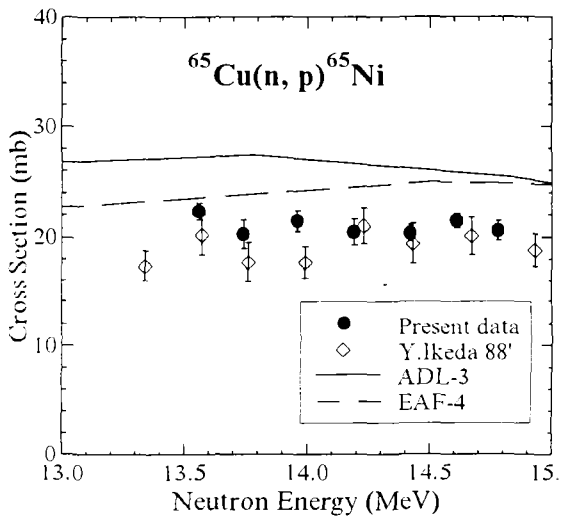


Fig. 5.20.

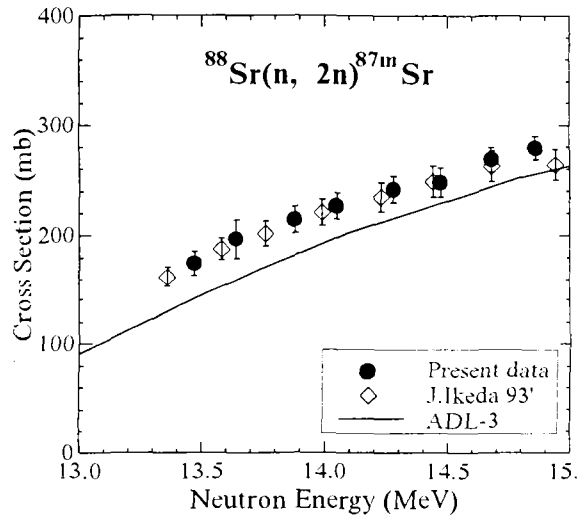


Fig. 5.23.

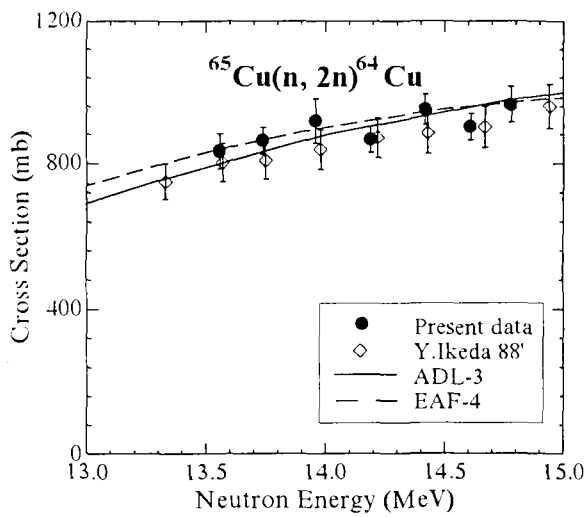


Fig. 5.21.

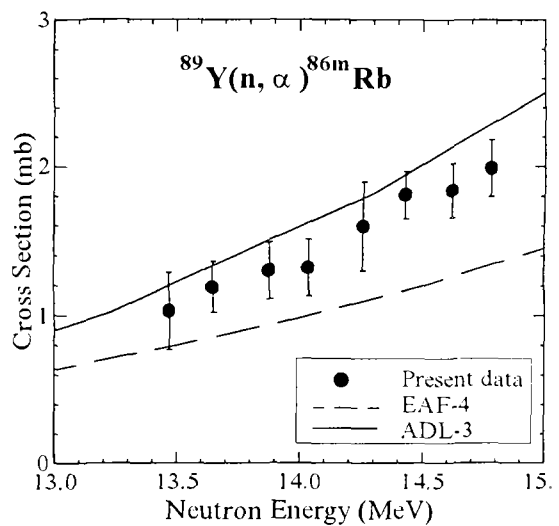


Fig. 5.24.

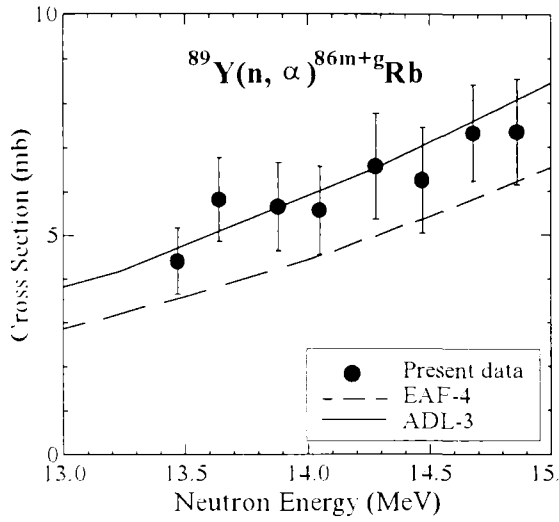


Fig. 5.25.

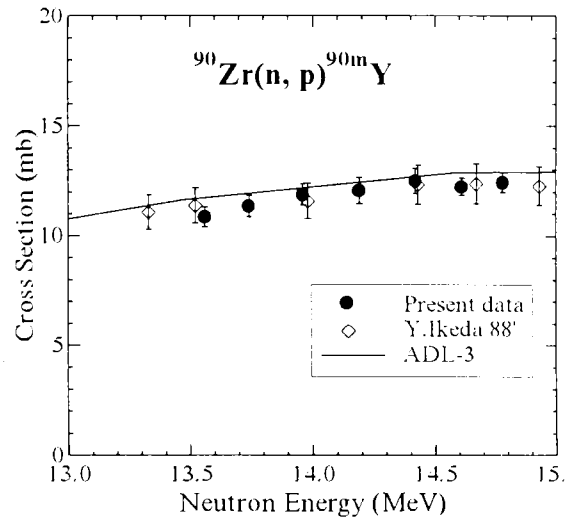


Fig. 5.28.

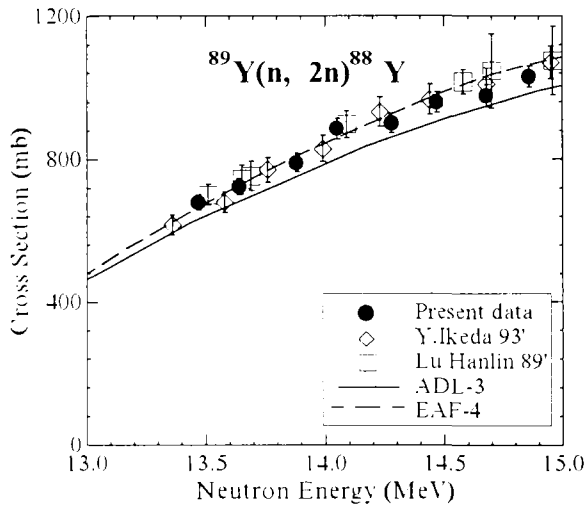


Fig. 5.26.

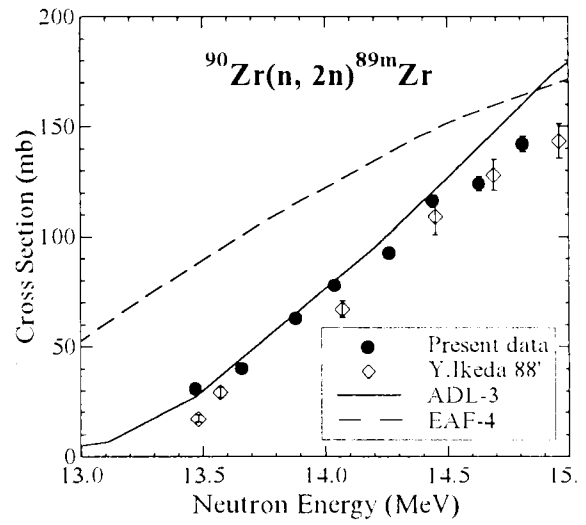


Fig. 5.29.

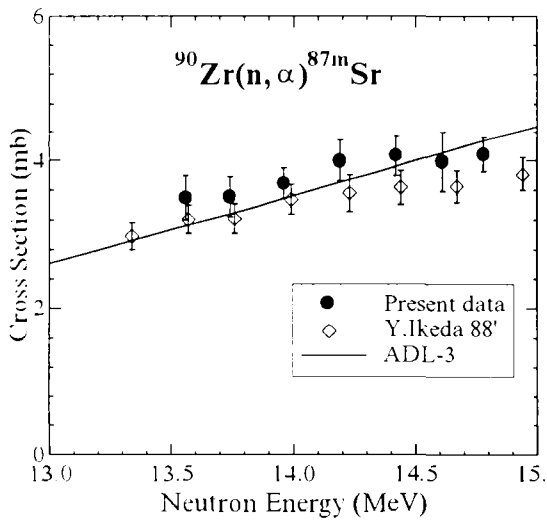


Fig. 5.27.

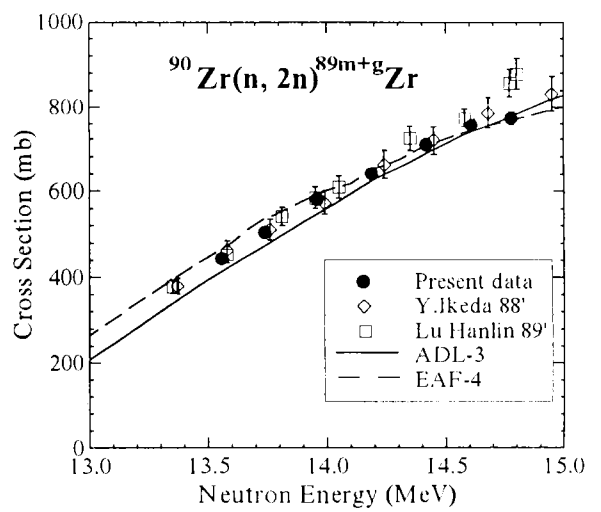


Fig. 5.30.

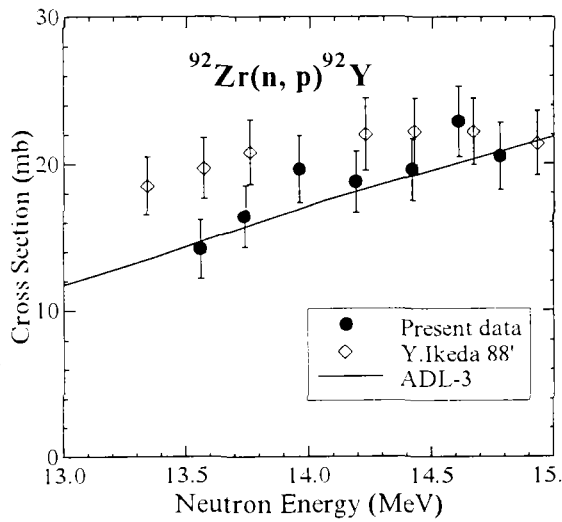


Fig. 5.31.

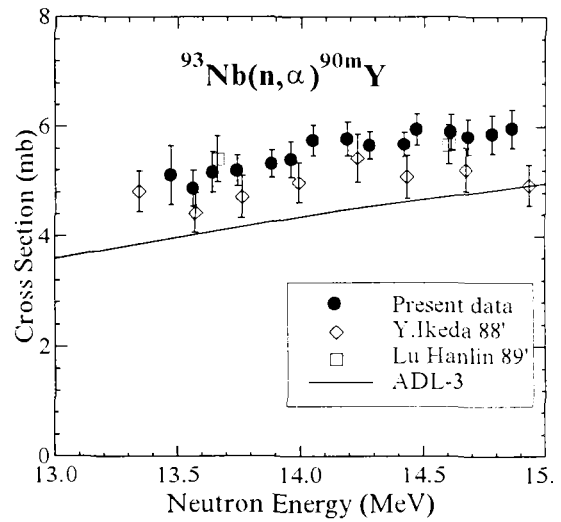


Fig. 5.34.

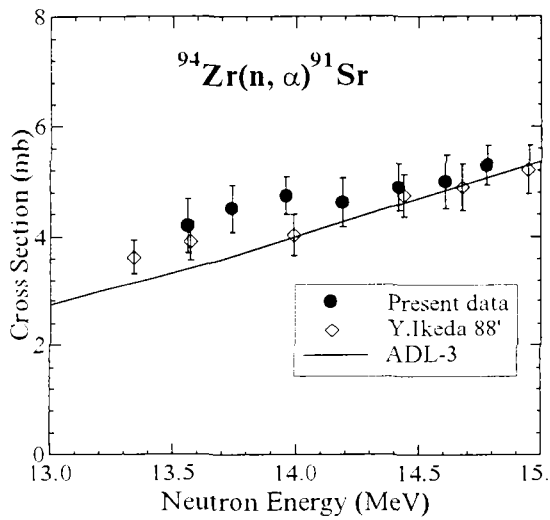


Fig. 5.32.

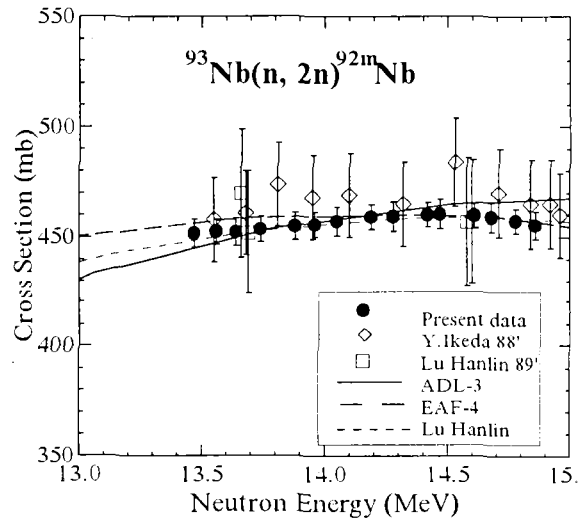


Fig. 5.35.

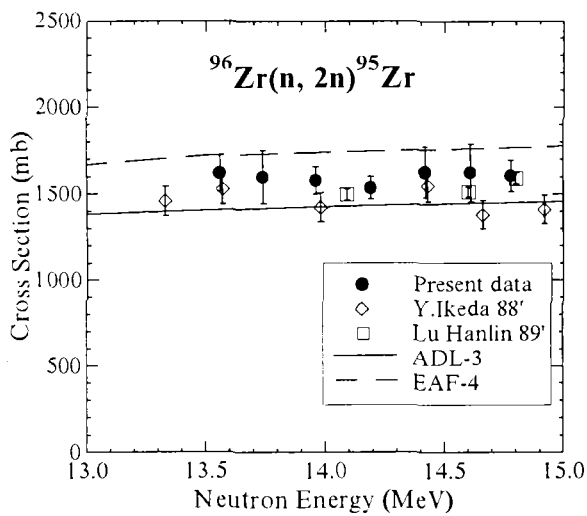


Fig. 5.33.

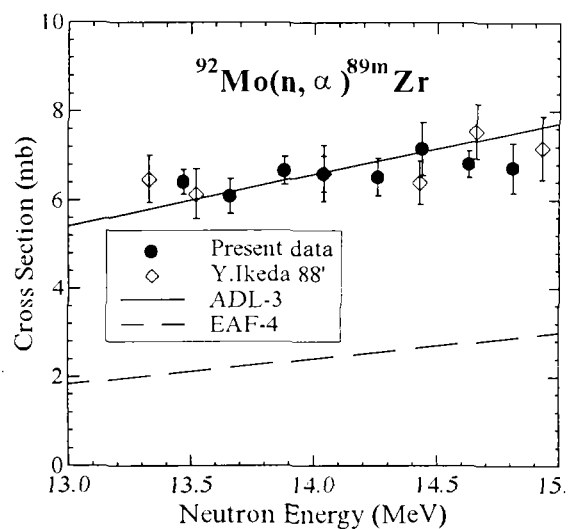


Fig. 5.36.

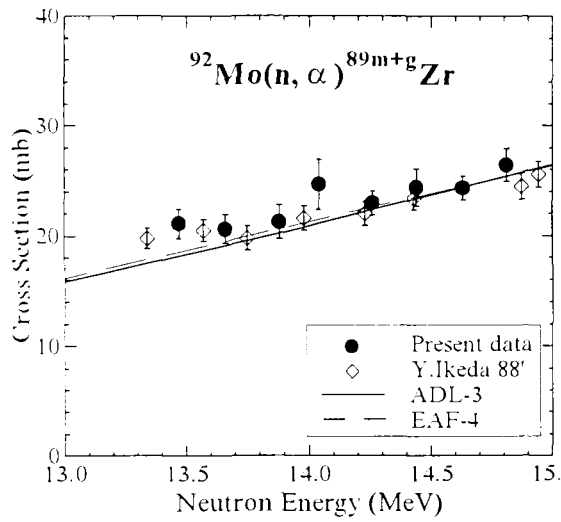


Fig. 5.37.

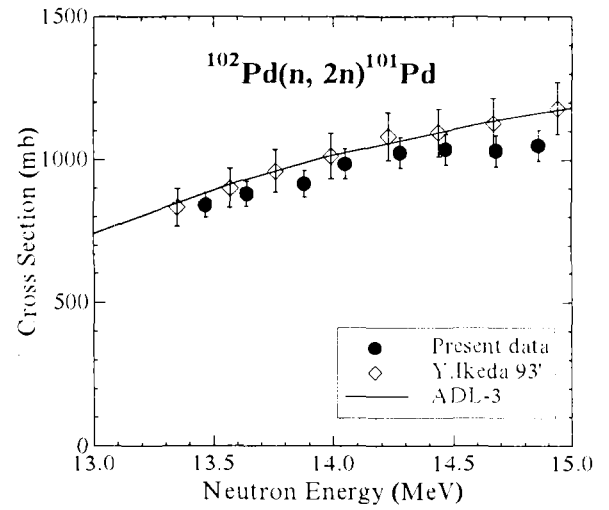


Fig. 5.40.

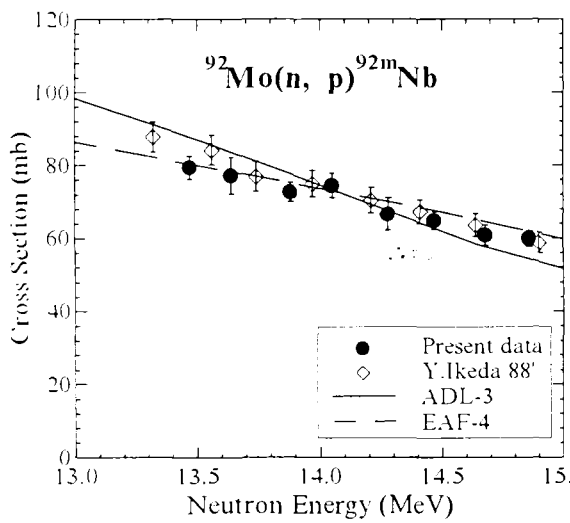


Fig. 5.38.

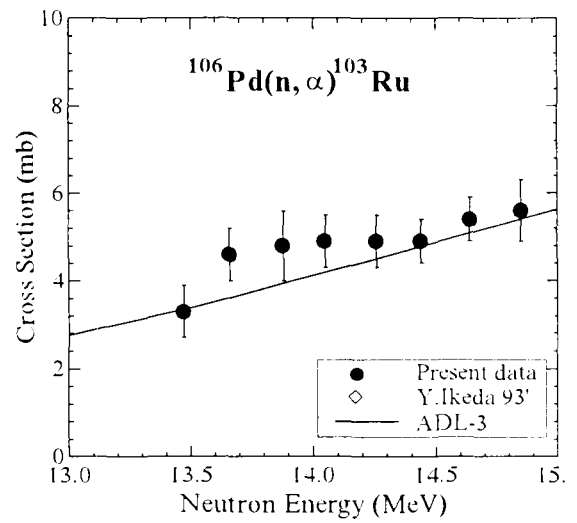


Fig. 5.41.

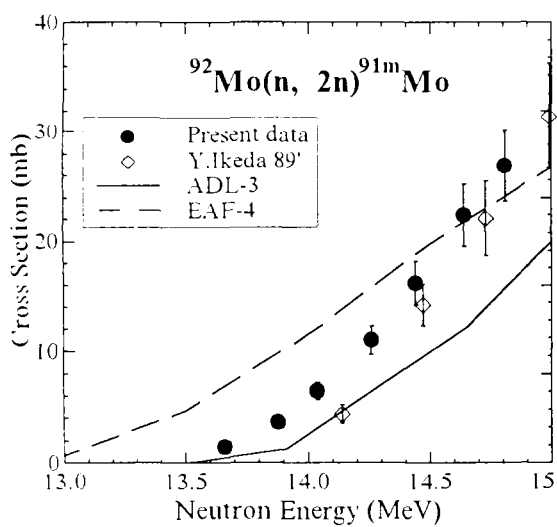


Fig. 5.39.

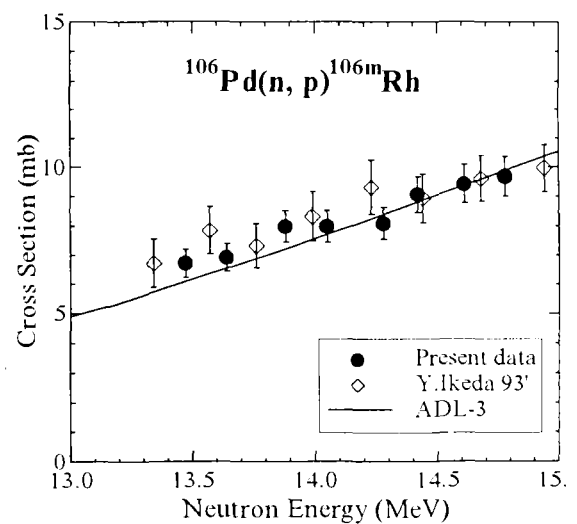


Fig. 5.42.

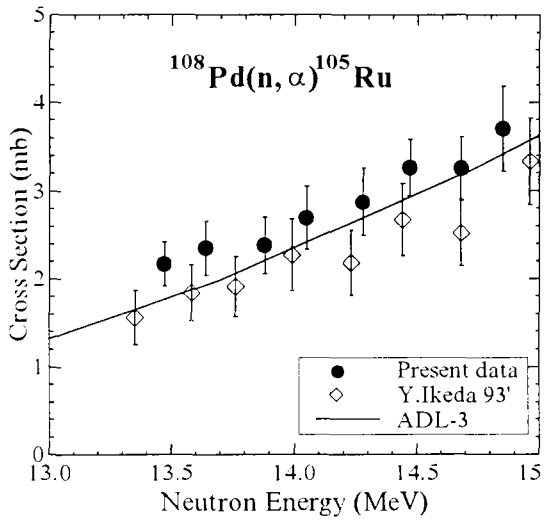


Fig. 5.43.

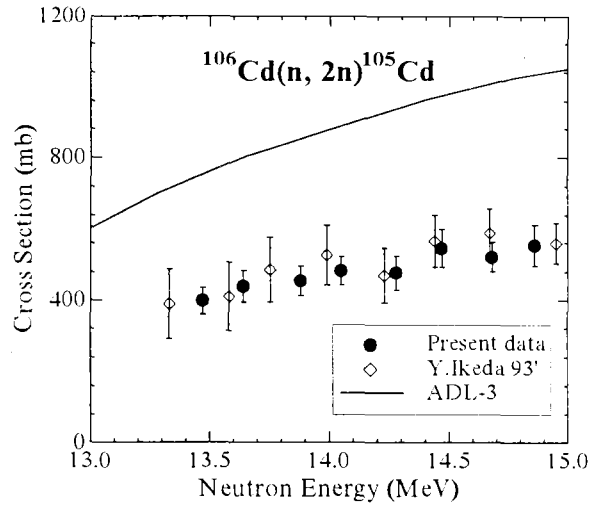


Fig. 5.46.

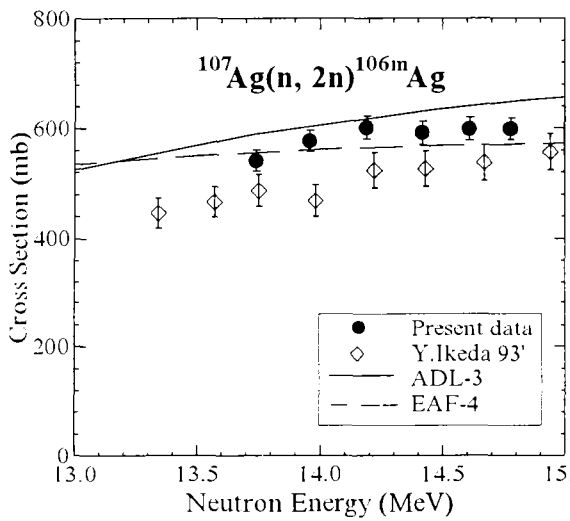


Fig. 5.44.

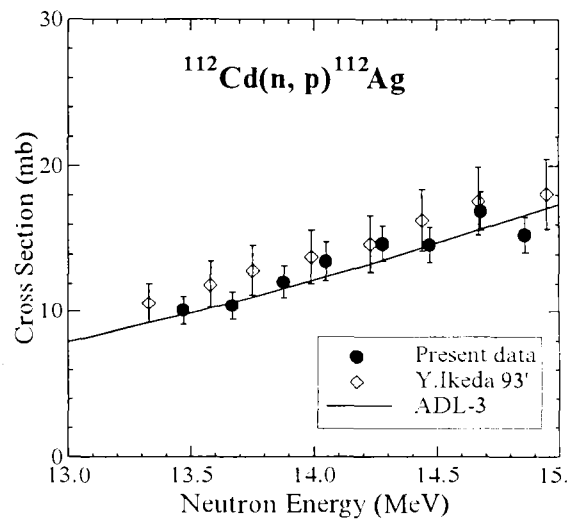


Fig. 5.47.

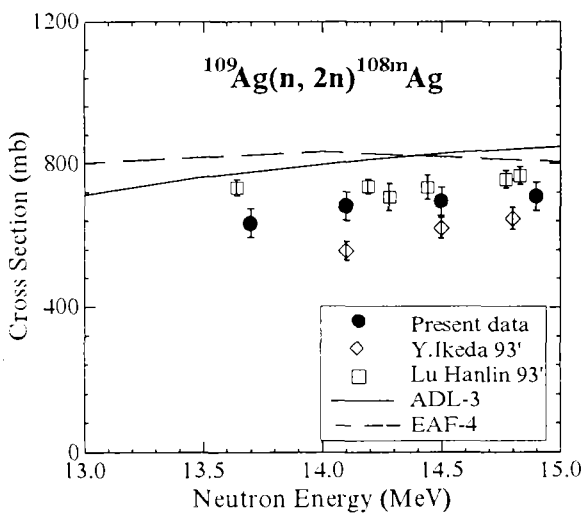


Fig. 5.45.

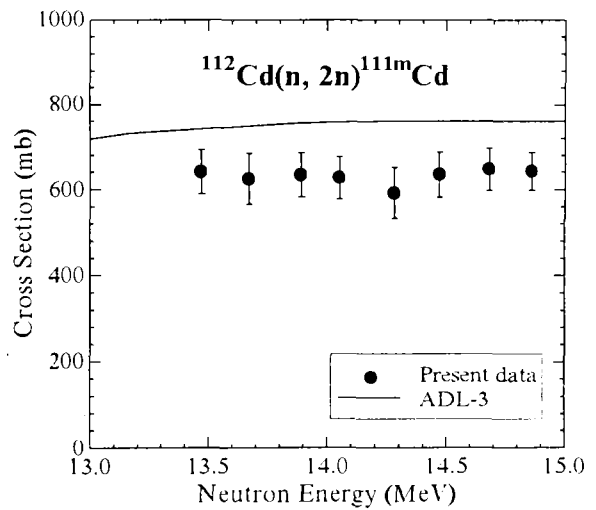


Fig. 5.48.

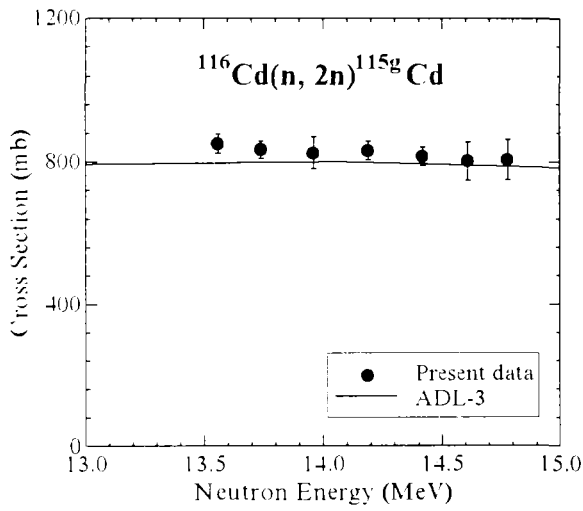


Fig. 5.49.

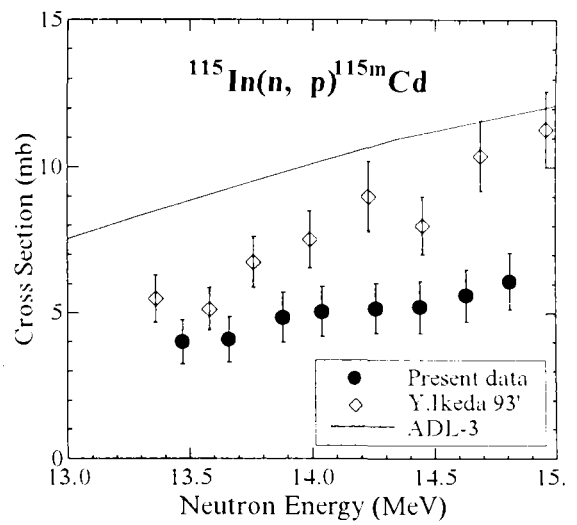


Fig. 5.52.

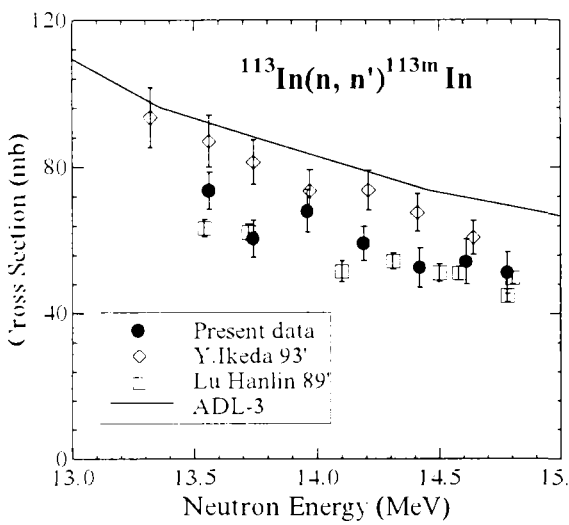


Fig. 5.50.

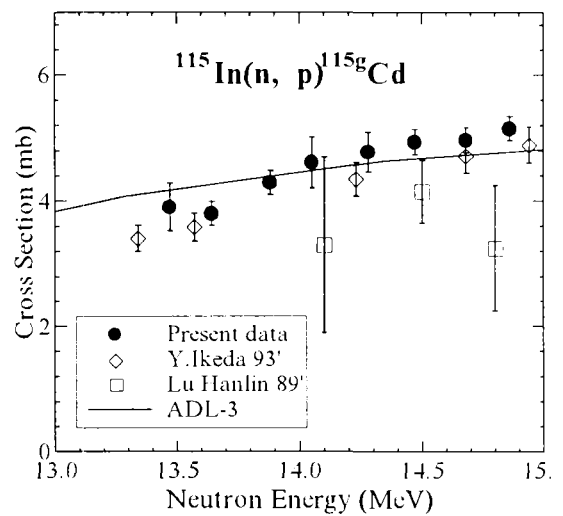


Fig. 5.53.

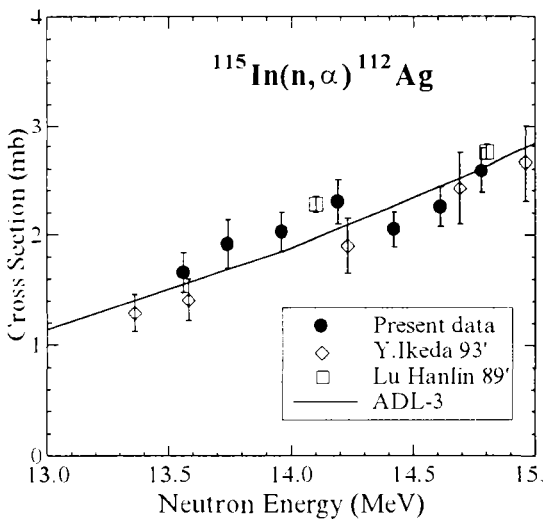


Fig. 5.51.

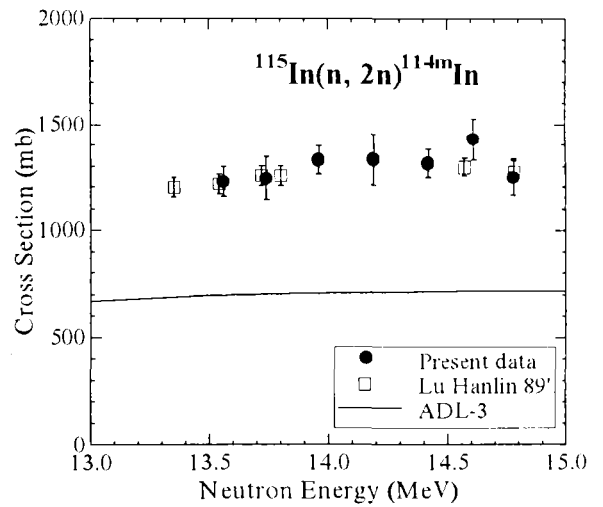


Fig. 5.54.

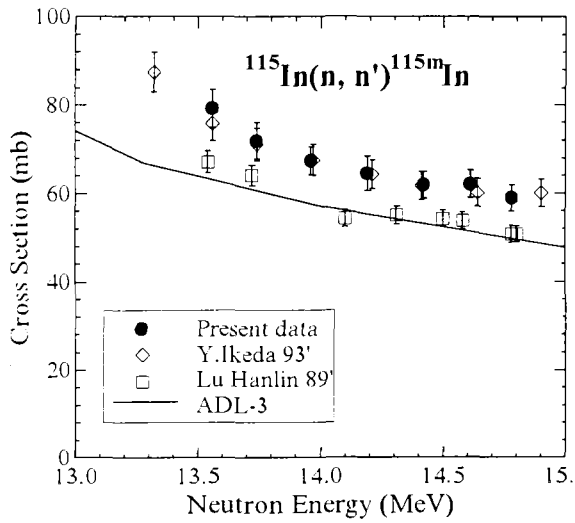


Fig. 5.55.

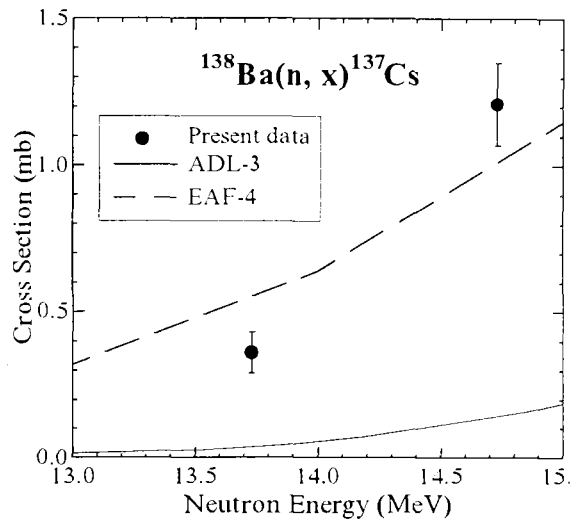


Fig. 5.58.

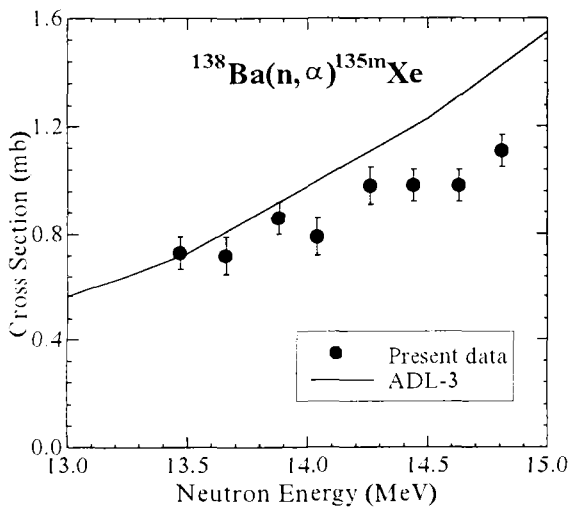


Fig. 5.56.

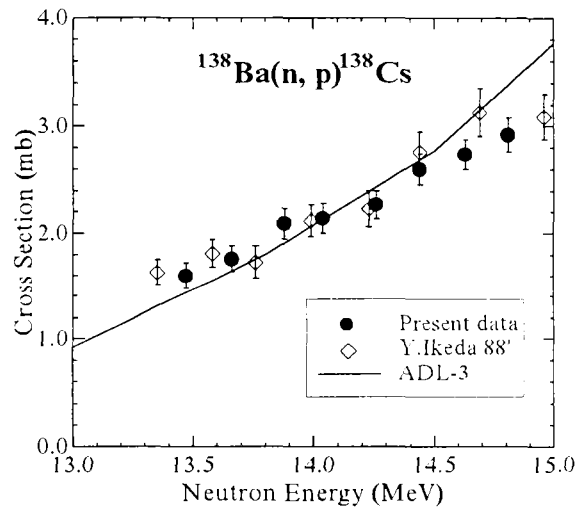


Fig. 5.59.

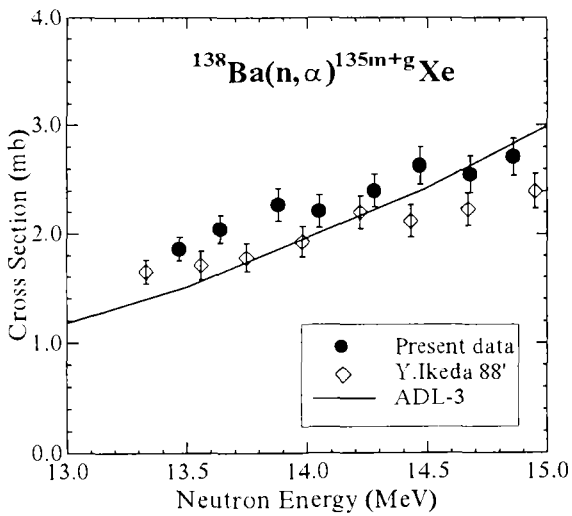


Fig. 5.57.

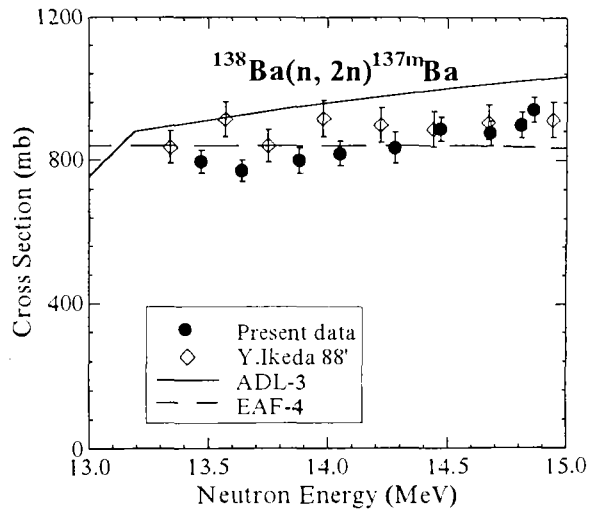


Fig. 5.60.

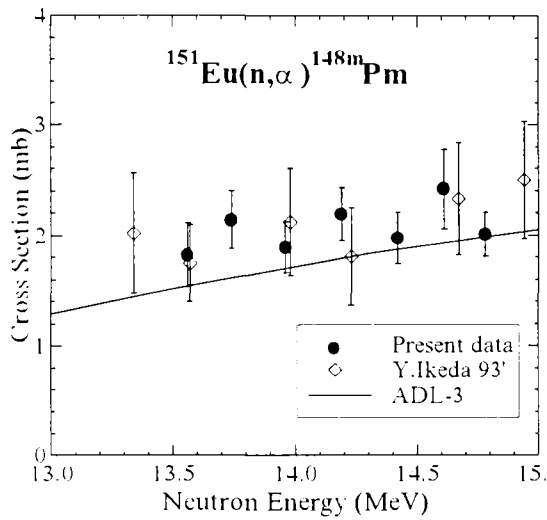


Fig. 5.61.

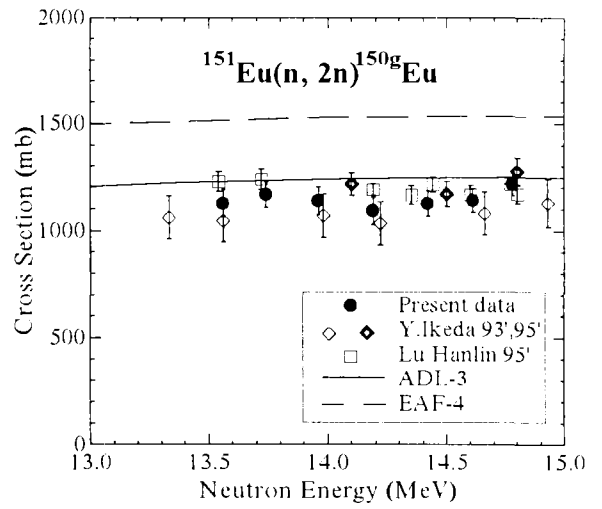


Fig. 5.64.

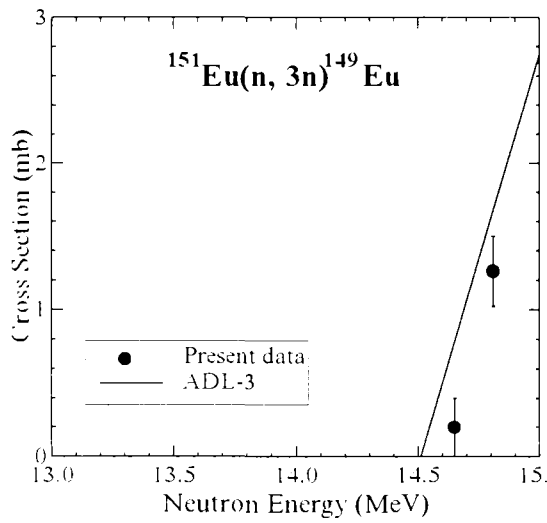


Fig. 5.62.

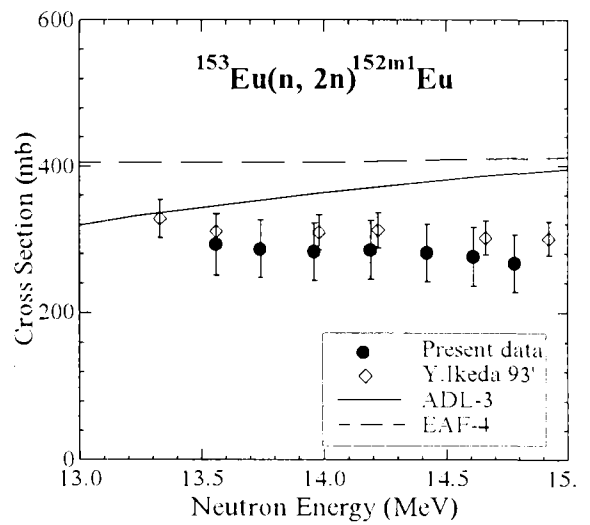


Fig. 5.65.

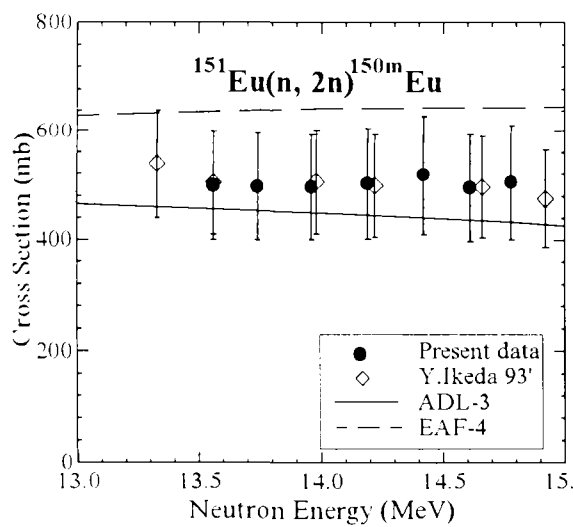


Fig. 5.63.

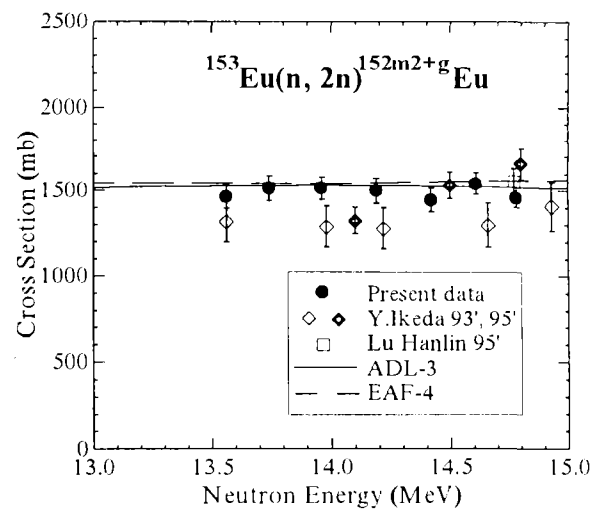


Fig. 5.66.

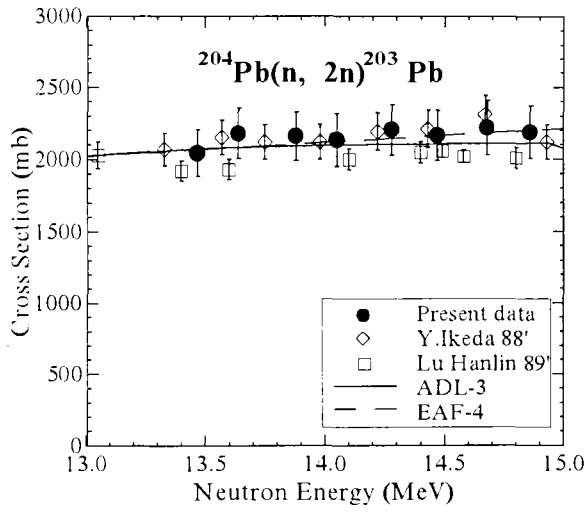


Fig. 5.67.

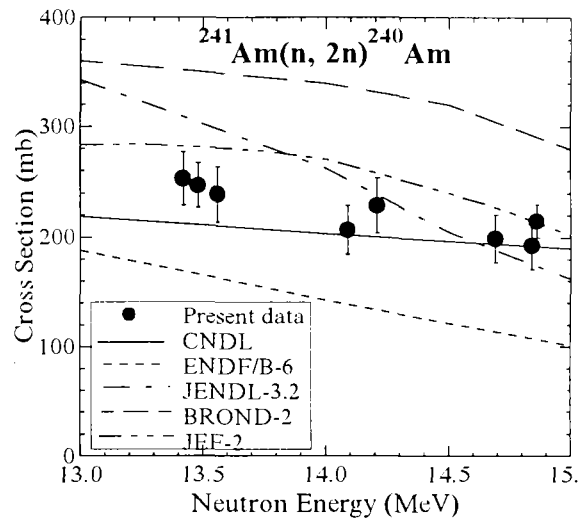


Fig. 5.69

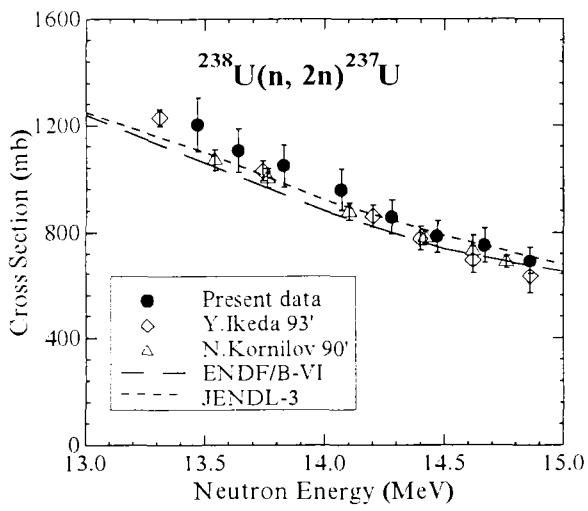


Fig. 5.68.

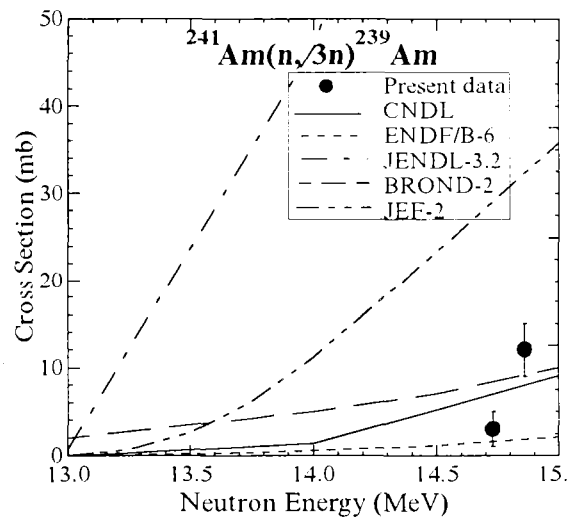


Fig. 5.70

Table 5.71. List of reactions for which cross section were measured and presented in this work.

Reaction	Q [MeV]	I_{init}	I_{final}	σ [mb]	$d\sigma/dE$
				En=14.1 MeV	[mb/MeV]
$^{23}\text{Na}(n, 2n)^{22}\text{Na}$	-12.42	3/2+	3+	19 (2)	27 (2)
$^{27}\text{Al}(n, p)^{27}\text{Mg}$	-1.83	1/2+	1/2+	71.0 (1.5)	-10 (2)
$^{39}\text{K}(n, 2n)^{38}\text{K}$	-13.08	3/2+	3+	1.53 (0.13)	2.53 (0.23)
$^{41}\text{K}(n, \alpha)^{38}\text{Cl}$	-0.12	3/2+	2-	34.7 (1.6)	-5.6 (1.3)
$^{41}\text{K}(n, p)^{41}\text{Ar}$	-1.71	3/2+	7/2-	51.9 (1.8)	-6.2 (1.6)
$^{51}\text{V}(n, \alpha)^{48}\text{Sc}$	-2.06	7/2-	6+	16.0 (0.7)	3.0 (0.4)
$^{55}\text{Mn}(n, \alpha)^{52}\text{V}$	-0.62	5/2-	3+	22.2 (1.0)	1.9 (0.9)
$^{55}\text{Mn}(n, 2n)^{54}\text{Mn}$	-10.23	5/2-	3+	690 (25)	142 (12)
$^{56}\text{Fe}(n, p)^{56}\text{Mn}$	-2.91	0+	3+	112 (4)	-10 (3)
$^{59}\text{Co}(n, \alpha)^{56}\text{Mn}$	0.33	7/2-	3+	31.5 (0.9)	0.6 (0.3)
$^{59}\text{Co}(n, p)^{59}\text{Fe}$	-0.78	7/2-	3/2-	50.3 (1.8)	-5.7 (1.5)
$^{59}\text{Co}(n, 2n)^{58\text{m}}\text{Co}$	-10.48	7/2-	5+	434 (9)	86 (14)
$^{59}\text{Co}(n, 2n)^{58\text{m-g}}\text{Co}$	-10.45	7/2-	2+	662 (10)	127 (22)
$^{58}\text{Ni}(n, np)^{57}\text{Co}$	-5.95	0+	7/2-	610 (20)	120 (20)
$^{58}\text{Ni}(n, p)^{58\text{m}}\text{Co}$	0.38	0+	5+	193 (4)	-64 (8)
$^{58}\text{Ni}(n, p)^{58\text{m-g}}\text{Co}$	0.40	0+	2+	349 (5)	-106 (11)
$^{58}\text{Ni}(n, 2n)^{57}\text{Ni}$	-12.22	0+	3/2-	236 (5)	19.8 (1.1)
$^{60}\text{Ni}(n, p)^{60}\text{Co}$	-2.04	0+	5+	155 (4)	-18 (5)
$^{63}\text{Cu}(n, \alpha)^{60}\text{Co}$	1.71	3/2-	5+	45.3 (0.8)	-2.9 (0.4)
$^{65}\text{Cu}(n, p)^{65}\text{Ni}$	-1.35	3/2-	5/2-	21.3 (0.7)	-0.9 (0.9)
$^{65}\text{Cu}(n, 2n)^{64}\text{Cu}$	-9.91	3/2-	1+	888 (25)	80 (40)
$^{88}\text{Sr}(n, \alpha)^{85\text{m}}\text{Kr}$	-1.10	0+	1/2-	1.20 (0.7)	0.54 (0.07)
$^{88}\text{Sr}(n, 2n)^{87\text{m}}\text{Sr}$	-11.50	0+	1/2-	226 (10)	72 (6)
$^{89}\text{Y}(n, \alpha)^{86\text{m}}\text{Rb}$	0.13	1/2-	6-	1.48 (0.12)	0.75 (0.10)
$^{89}\text{Y}(n, \alpha)^{86\text{m-g}}\text{Rb}$	0.69	1/2-	2-	6.0 (0.6)	1.9 (0.5)
$^{89}\text{Y}(n, 2n)^{88}\text{Y}$	-11.48	1/2-	4-	851 (25)	260 (30)
$^{90}\text{Zr}(n, \alpha)^{87\text{m}}\text{Sr}$	1.36	0+	1/2-	3.79 (0.15)	0.54 (0.15)
$^{90}\text{Zr}(n, p)^{90\text{m}}\text{Y}$	-2.18	0+	7+	11.8 (0.4)	1.2 (0.3)
$^{90}\text{Zr}(n, 2n)^{89\text{m}}\text{Zr}$	-12.56	0+	1/2-	82 (2)	83 (4)
$^{90}\text{Zr}(n, 2n)^{89\text{m-g}}\text{Zr}$	-11.97	0+	9/2+	607 (8)	283 (20)
$^{92}\text{Zr}(n, p)^{92}\text{Y}$	-2.83	0+	2-	18.3 (1.8)	5.6 (2.0)
$^{94}\text{Zr}(n, \alpha)^{91}\text{Sr}$	2.04	0+	5/2+	4.72 (0.30)	0.74 (0.18)
$^{96}\text{Zr}(n, 2n)^{95}\text{Zr}$	-7.85	0+	5/2+	1580 (50)	5 (6)
$^{93}\text{Nb}(n, \alpha)^{90\text{m}}\text{Y}$	4.24	9/2+	7+	5.52 (0.20)	0.73 (0.23)
$^{93}\text{Nb}(n, 2n)^{92\text{m}}\text{Nb}$	-8.97	9/2+	(2)+	457 (4)	5 (3)
$^{92}\text{Mo}(n, \alpha)^{89\text{m}}\text{Zr}$	3.12	0+	1/2-	6.6 (0.3)	0.4 (0.3)

$^{92}\text{Mo}(n, \alpha) ^{89\text{m}+\text{g}}\text{Zr}$	3.71	0+	9/2+	22.8 (0.8)	3.7 (1.1)
$^{92}\text{Mo}(n, p) ^{92\text{m}}\text{Nb}$	0.29	0+	(2)+	70.5 (1.5)	-14.6 (1.7)
$^{92}\text{Mo}(n, 2n) ^{91\text{m}}\text{Mo}$	-13.33	0+	1/2-	8.6 (1.0)	18.6 (2.7)
$^{102}\text{Pd}(n, 2n) ^{101}\text{Pd}$	-10.57	0+	(5/2)+	958 (40)	160 (50)
$^{106}\text{Pd}(n, \alpha) ^{103}\text{Ru}$	3.00	0+	3/2+	4.7 (0.5)	1.3 (0.5)
$^{106}\text{Pd}(n, p) ^{106\text{m}}\text{Rh}$	-2.90	0+	(6)+	8.1 (0.4)	2.3 (0.4)
$^{108}\text{Pd}(n, \alpha) ^{105}\text{Ru}$	2.06	0+	3/2+	2.77 (0.3)	1.02 (0.15)
$^{107}\text{Ag}(n, 2n) ^{106\text{m}}\text{Ag}$	-9.62	1/2-	6+	576 (15)	49 (21)
$^{109}\text{Ag}(n, 2n) ^{108\text{m}}\text{Ag}$	-7.25	1/2-	6+	668 (30)	60 (20)
$^{106}\text{Cd}(n, 2n) ^{105}\text{Cd}$	-10.86	0+	5/2+	480 (30)	100 (20)
$^{112}\text{Cd}(n, p) ^{112}\text{Ag}$	-3.18	0+	2(-)	13.1 (0.9)	4.7 (1.1)
$^{112}\text{Cd}(n, 2n) ^{111\text{m}}\text{Cd}$	-9.80	0+	11/2-	630 (40)	6.7 (2.1)
$^{116}\text{Cd}(n, 2n) ^{115\text{g}}\text{Cd}$	-8.70	0+	1/2+	828 (25)	-36 (10)
$^{113}\text{In}(n, n') ^{113\text{m}}\text{In}$	-0.39	9/2+	1/2-	61 (4)	-16 (7)
$^{115}\text{In}(n, \alpha) ^{112}\text{Ag}$	2.73	9/2+	2(-)	2.05 (0.14)	0.6 (0.2)
$^{115}\text{In}(n, p) ^{115\text{m}}\text{Cd}$	-0.84	9/2+	11/2-	4.92 (60)	1.46 (0.26)
$^{115}\text{In}(n, p) ^{115\text{g}}\text{Cd}$	-0.66	9/2+	1/2+	4.45 (0.15)	1.0 (0.2)
$^{115}\text{In}(n, 2n) ^{114\text{m}}\text{In}$	-9.23	9/2+	5+	1300 (50)	64 (80)
$^{115}\text{In}(n, n') ^{115\text{m}}\text{In}$	-0.34	9/2+	1/2-	67.5 (2.5)	-14 (3)
$^{138}\text{Ba}(n, \alpha) ^{135\text{m}}\text{Xe}$	3.35	0+	11/2-	0.88 (0.05)	0.28 (0.06)
$^{138}\text{Ba}(n, \alpha) ^{135\text{m}+\text{g}}\text{Xe}$	3.88	0+	3/2+	2.28 (0.05)	0.6 (0.1)
$^{138}\text{Ba}(n, x) ^{137}\text{Cs}$	-6.28*	0+	7/2+	0.68 (0.08)	0.85 (0.15)
$^{138}\text{Ba}(n, 2n) ^{137\text{m}}\text{Ba}$	-9.27	0+	11/2-	833 (30)	100 (25)
$^{138}\text{Ba}(n, p) ^{138}\text{Cs}$	-4.59	0+	3-	2.21 (0.10)	1.0 (0.1)
$^{151}\text{Eu}(n, \alpha) ^{148\text{m}}\text{Pm}$	7.73	5/2+	6-	2.0 (0.2)	0.11 (0.24)
$^{151}\text{Eu}(n, 3n) ^{149}\text{Eu}$	-14.35	5/2+	5/2+	*	
$^{151}\text{Eu}(n, 2n) ^{150\text{m}}\text{Eu}$	-7.98	5/2+	0-	500 (80)	6.4 (9.0)
$^{151}\text{Eu}(n, 2n) ^{150\text{g}}\text{Eu}$	-7.94	5/2+	5(-)	1143 (40)	36 (55)
$^{153}\text{Eu}(n, 2n) ^{152\text{m}1}\text{Eu}$	-8.60	5/2+	0-	282 (30)	-17 (5)
$^{153}\text{Eu}(n, 2n) ^{152\text{m}2+\text{g}}\text{Eu}$	-8.55	5/2+	3-	1490 (60)	-6 (50)
$^{204}\text{Pb}(n, 2n) ^{203}\text{Pb}$	-8.39	0+	5/2-	2150 (150)	-30 (12)
$^{238}\text{U}(n, 2n) ^{237}\text{U}$	-6.15	0+	1/2+	940 (60)	-343 (25)
$^{241}\text{Am}(n, 2n) ^{240}\text{Am}$	-6.63	5/2-	(3-)	217 (14)	-39 (14)
$^{241}\text{Am}(n, 3n) ^{239}\text{Am}$	-12.60	5/2-	(5/2)-	*	

* - the procedure of approximation the data near the threshold is not correct.

6. MEASUREMENT OF ISOMERIC RATIOS

Isomeric ratios are a rather sensitive test for parameters used in calculation of nuclear reaction cross sections. Since there is no universal systematics available for isomeric ratios, an experimental study of them is an important task. However, until recently, only few such investigations had been performed. In the present work the data for eight isomeric ratios are given. Six ratios are derived from the separate measurement of cross sections leading to population of ground and metastable states. For two others, the $^{59}\text{Co}(n, 2n)^{58\text{m.g}}\text{Co}$ and $^{58}\text{Ni}(n, p)^{58\text{m.g}}\text{Co}$, a special method was developed that enabled the determination of isomeric ratios directly and with good accuracy. In this measurement, six gamma spectrometers from five different laboratories in the Khlopin Radium Institute were involved.

Isomeric ratios are presented in Figs. 6.1 - 6.9 where they are compared with the ADL-3 and EAF-4 evaluations. It could be noted that, on the whole, the data agree better with the ADL-3 evaluation.

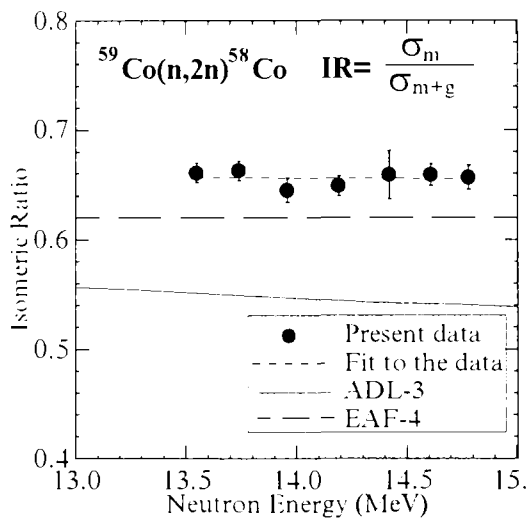


Fig. 6.1.

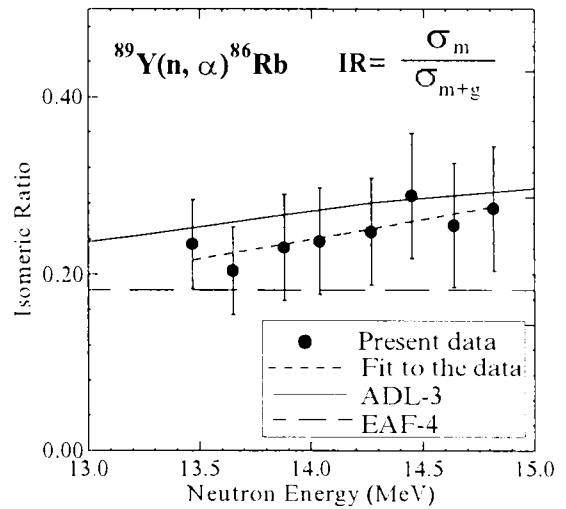


Fig. 6.3.

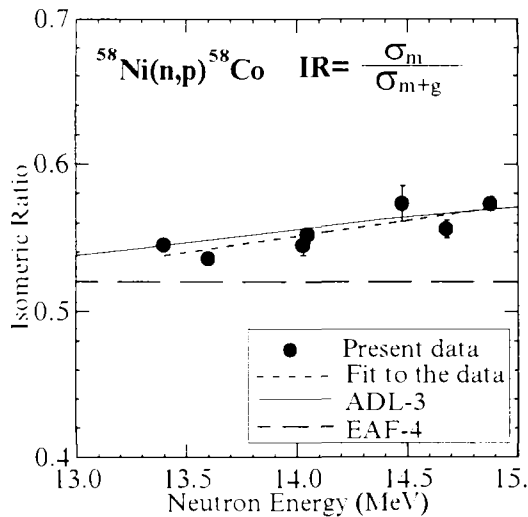


Fig. 6.2.

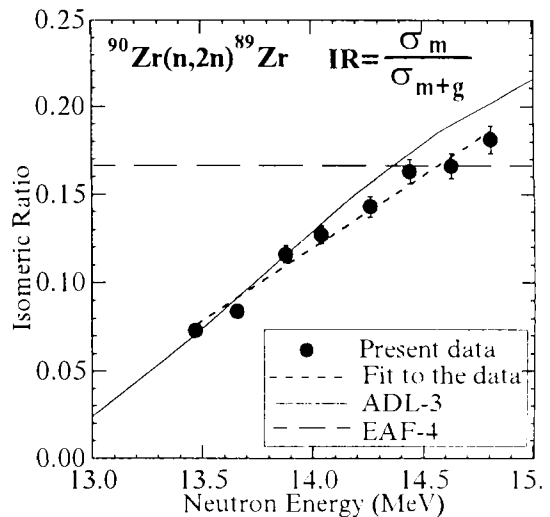


Fig. 6.4.

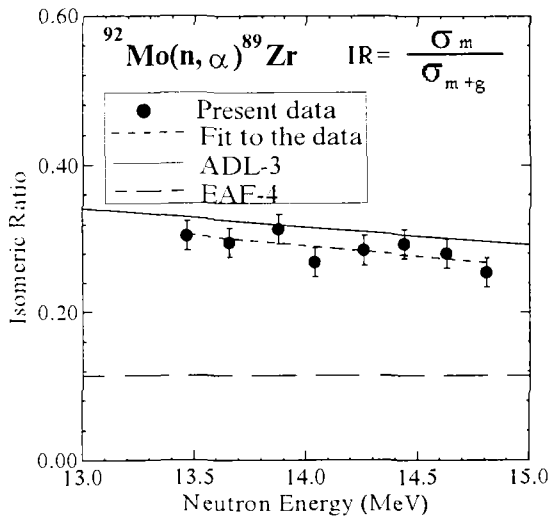


Fig. 6.5.

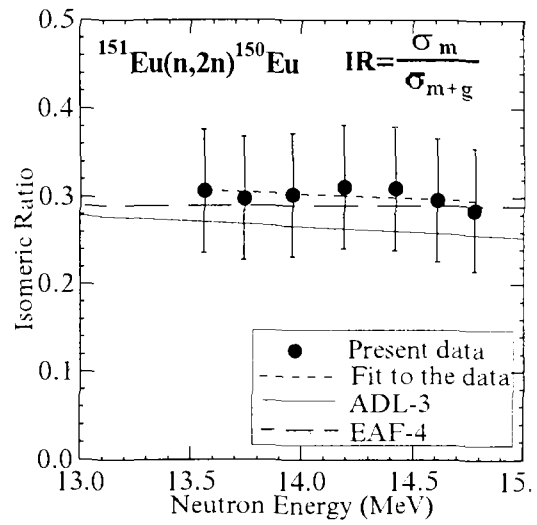


Fig. 6.8.

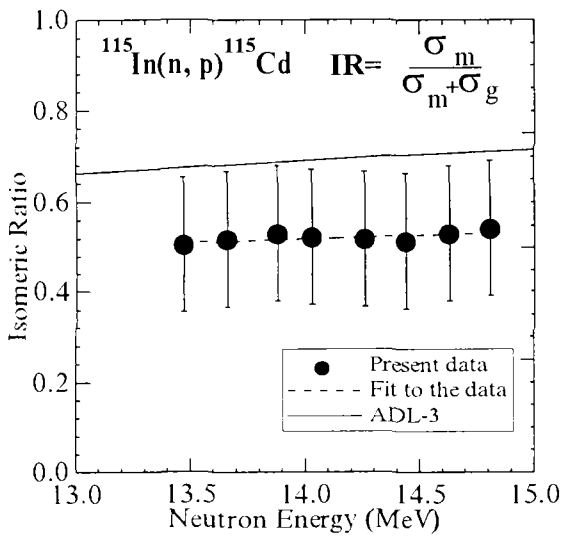


Fig. 6.6.

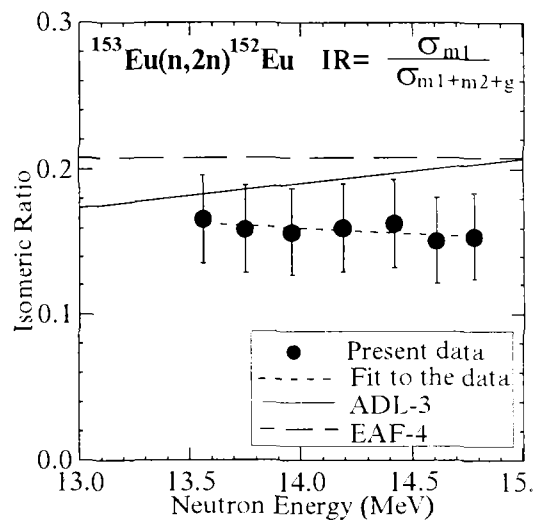


Fig. 6.9.

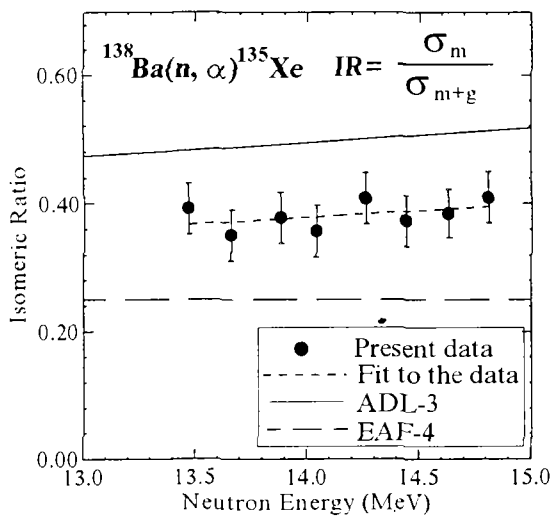


Fig. 6.7.

7. CONCLUSION

The results of systematic cross section measurement made for 70 nuclear reactions in neutron energy range of 13.4 - 14.9 are presented in the paper. The main part of the data were obtained under standard, rigidly fixed conditions. Their accuracy is mostly of order 2 - 5 %. The data are compared with evaluations and sets of experimental data obtained recently, for example [1, 2, 3]. Although results of comparison of the data and evaluations are strictly individual, nevertheless, the general tendency could be noted also. It is, in opinion of authors, a better agreement between the latest experimental data than between experiments and evaluations. Sometimes this difference is essential, as for instance, for $^{93}\text{Nb}(n, \alpha)^{90\text{m}}\text{Y}$, $^{92}\text{Mo}(n, \alpha)^{89\text{m}}\text{Zr}$, $^{106}\text{Cd}(n, 2n)^{105}\text{Cd}$, $^{115}\text{In}(n, 2n)^{114\text{m}}\text{In}$, $^{153}\text{Eu}(n, 2n)^{152\text{m1}}\text{Eu}$

The isomeric ratios measured in the present work showed a better agreement with the evaluation ADL-3 in which complex nuclear models were involved.

The authors hope that the data obtained will be used for further progress in evaluations of nuclear data.

ACKNOWLEDGMENTS

Authors express the sincere acknowledgment to B.K. Seleznev and A.V.Orlovskiy for reliable work of the Neutron Generator NG-400, B.P.Gavrilov for sample preparation and help in the work, and V.M.Saidgareev for supervising of electronic systems. The authors are very grateful to Dr. D.Smith (ANL, USA), Dr. Y.Ikeda (JAERI, Japan), Prof. H.Vonach (IRK, Austria) and Prof. J.Csikai (Debrecen, Hungary) for their active interest, useful discussions and immediate participation in some measurements.

REFERENCES

1. Yujiro Ikeda et al. Activation Cross Section Measurements for Fusion Reactor Structural Materials at Neutron Energy from 13.3 to 15.0 MeV Using FNS Facility: JEARI 1312, 1988.
2. Chikara Konno et al. Activation Cross Section Measurements at Neutron Energy from 13.3 to 14.9 MeV Using the FNS Facility: JEARI 1329, 1993.
3. Zhao Wenrong et al. Compilation of Measurements and Evaluations of Nuclear Activation Cross Sections for Nuclear Data Application. // INDC (CRP)-16, Vienna, IAEA, 1989.
4. A.H.Wapstra, G.Andi, R.Hoekstra. // Atomic Data and Nuclear Data Tables, 1988. v.38, No. 2, pp. 290-393.
5. A.B.Pashchenko. Reaction Cross Sections Induced by 14.5 MeV and by Cf-252 and U-235 Fission Spectrum Neutrons. // INDC(CCP)-323/L, 1991.
6. P.Ekstroem and L.Spanier. The ENSDF Radioactivity Data Base for IBM-PC and Computer Network Access. // IAEA-NDS-118, 1989.
7. T.V.Ryves. A Simultaneous Evaluation of Some Important Cross Sections at 14.70 MeV. // Europ. Appl. Res. Rep. Nucl. Sci. Techn., 1989. v.7, p. 1241.
8. M.Wagner, H.Vonach, A.Pavlik et al. Evaluation of Cross Sections for 14 Important Neutron-Dosimetry Reactions. // Physics Data, 1990. No.13-5.
9. V.A.Jakovlev. An analytical expression for energy spectrum of fast neutrons at the finite geometry of experiment. Prog. Rep. of KRI-211, Moscow, CNIIAtominform, 1988 (In Russian).
10. O.T.Grudzevich et al. Catalog of the ADL-3 library // Problems of Nuclear Science and Technique. Ser. Nuclear Constants.-No.3-4. p.3. (1993) (In Russian).
11. Comparison of Activation Cross Section Measurements and Experimental Techniques for Fusion Reactor Technology / Proc. of the IAEA Specialists' Meeting held at the Tokai Research Establishment, JAERI, Japan, 15-17 November 1993. Prepared by A.B.Pashchenko, 1994. Report INDC(NDS)-301.
12. Activation Cross Sections for the Generation of Long-lived Radionuclides of Importance in Fusion Reactor Technology / Proc. of the IAEA Consultants' Meeting held at Argonne National Laboratory, Argonne, USA, 11-12 September 1989. Edited by Wang DaHai, 1990. Report INDC(NDS)-232/L.
13. Activation Cross Sections for the Generation of Long-lived Radionuclides of Importance in Fusion Reactor Technology / Proc. of the IAEA Consultants' Meeting held at the V.G.Khlopin Radium Institute, St. Petersburg, Russia, 19-23 June 1995. Prepared by A.B.Pashchenko, 1995 Report INDC(NDS)-340.
14. V.A.Konshin. Consistent Calculation of Fast Neutron Induced Fission, (n, 2n) and (n, 3n) Cross Sections for 71 Isotopes of Th, Pa, U, Np, Pu, Am, Cm, Bk and Cf: JEARI-Research 95-010. 1995.

Nuclear Data Section
International Atomic Energy Agency
P.O. Box 100
A-1400 Vienna
Austria

e-mail, INTERNET: SERVICES@IAEAND.IAEA.OR.AT
fax: (+43-1) 20607
cable: INATOM VIENNA
telex: 1-12645 atom a
telephone: (+43-1) 2060-21710

online: TELNET or FTP: IAEAND.IAEA.OR.AT
username: IAEANDS for interactive Nuclear Data Information System
username: ANONYMOUS for FTP file transfer
For users with web-browsers: <http://www-nds.iaea.or.at>
